Analytical Methods

Accepted Manuscript

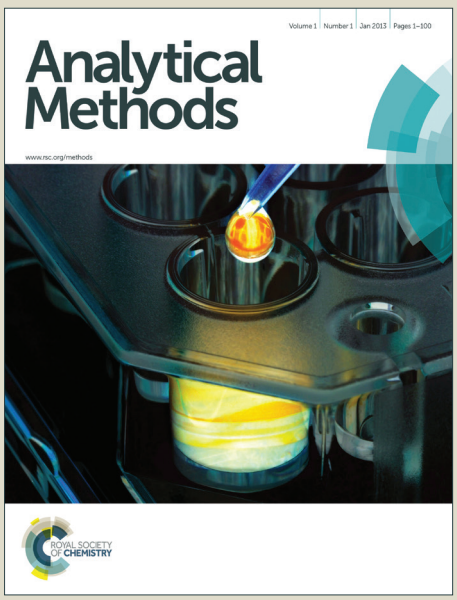

ROYAL SOCIETY OF CHEMISTRY

www.rsc.org/methods

[Submitted as a Critical Review to *Analytical Methods*]

Atomic Force Microscopy-based Bioanalysis for the Study of Disease

Kirstin C. Morton and Lane A. Baker*

Department of Chemistry

Indiana University

800 E Kirkwood Avenue

Bloomington, IN 47405

*Author to whom correspondence should be addressed.

e-mail: lanbaker@indiana.edu; voice: 812 856-1873

Submitted XX

ABSTRACT

Atomic force microscopy (AFM) has emerged as a robust and well-tested method to image and probe living systems. Atomic force microscopy, one of many types of scanning probe microscopies, but has proven useful for the investigation of disease states and single cell analysis, as a result of high spatial resolution, sensitivity and diversity of operational modes. In addition, AFM can be easily hybridized with secondary techniques, such as fluorescence microscopy, to provide correlated information related to biological samples. This review aims to describe the operation of AFM related to the study of disease states and single cell analysis, and to serve as an overview of recent advances in this subject area. In addition, force spectroscopy, force mapping and relevant hybrid AFM instrumentation will be discussed.

Keywords: Atomic force microscopy (AFM), scanning probe microscopy (SPM), single cell analysis, bioanalytical, disease

1. INTRODUCTION

Single cell analysis provides one method to investigate the relationship between molecular biology at the cellular level and pathogenesis. For instance, nanoscale morphological changes of a single cell in an aggregate of cells or tissue specimen can help ascertain the effects of chemical or environmental stimuli, such as the exposure of skin to UV light.[1, 2] Single cell analysis is often used to characterize heterogeneity within a cell, virus, protein or tissue sample with mass spectrometry,[3] chromatography,[4] or vibrational spectroscopy.[5] To date, most analyses do not correlate physical and chemical information.[6] Besides the importance of tissue and cells morphology in disease research, evidence has emerged to suggest a strong link between the mechanical properties of cells and tissues with pathogenic states.[1, 7-14] Thus, methods that perform concomitant measurements of chemical/biochemical characteristics with physical properties present considerable opportunities in biomedical research.

Arguably, the most useful bioanalytical method to probe sub-micrometer cellular dynamics, mechanical properties and topography is the atomic force microscope (AFM). Atomic force microscopy is a versatile scanning probe microscopy (SPM) technique that has evolved beyond high-resolution imaging to include chemical/physical characterizations.[15] For instance, AFM has been used to manipulate single DNA molecules,[16] or to determine the Young's moduli of soft biological specimens.[8, 17, 18] Atomic force microscopy is well suited to investigation of biological samples, as image collection can be performed in physiological conditions without labeling or extensive sample preparation.[19] Furthermore, AFM can be hybridized with additional instruments, such as wide-field fluorescence microscopy,[20] confocal microscopy,[21] mass

spectrometry,[22] and Raman spectroscopy,[23] all of which add chemical and physical information to measurements made.

Significant efforts have been made to correlate tissue and cellular studies performed by AFM with the pathology of disease. In an effort to illustrate the depth and breadth of the studies related to disease research, selected disease categories with literature references are listed in **Table 1**, Excellent reviews related to general AFM advances in biology and biophysics have been published.[14, 24-31] Here we provide a brief background into the operating principles of AFM, followed by a review of studies related to single cell analysis and associated experiments in the broad view of human disease research. Progression of single cell analysis by AFM with respect to three areas is considered: (1) high-resolution topographical imaging, (2) force spectroscopy and mapping, and (3) hybrid AFM instrumentation. Finally, future prospects in these areas will be analyzed.

2. BIOANALYSIS WITH AFM

2.1 Operating Principles of AFM. Atomic force microscopy relies on the detection of attractive or repulsive surface forces (e.g., van der Waals (vdW) forces) by a tip that is attached to a flexible cantilever:

$$F_{vdW} = \frac{A_H * r}{6 * z} \qquad \textbf{(eq. 1)}^{32}$$

where F_{vdW} is the vdW force, A_H is the Hamaker constant for the given system, r is tip radius of curvature, and z is the tip-substrate distance.

The basic instrumental setup of an AFM is illustrated in **Figure 1a**, where a sharp tip at the end of a flexible cantilever is raster scanned via a piezoelectric positioning

system across a sample surface. The AFM cantilever can be thought of as a flexible spring, with a spring constant, k_N, which can be approximated by Hooke's law, and a resonance frequency, f_o. Forces that affect the cantilever and tip close to a surface include electrostatic forces (~100 nm from the surface), electrical double layer (EDL) forces (~100 nm from an electrode), vdW forces (~10 nm from the surface), or forces that are chemical in nature (*e.g.*, hydrogen bonding, ~0.2 nm from the surface).[32-34] As the tip is approached to the surface, an overall attractive (negative) force is experienced by the tip, which steadily decreases as the two are brought closer together. Eventually, the electrostatic repulsion between the tip and surface is so large that a net repulsive (positive) force is experienced by the tip (**Figure 1b**). Atomic force microscopy can operate with the tip-sample interaction in either the attractive or repulsive potential energy regime, where changes in the force experienced by the cantilever are utilized to control tip-substrate position. Force curves will be analyzed in more detail in **Section 4**.

A feedback mechanism is used to control the probe position as the surface is scanned. For instance, in contact-mode imaging feedback is controlled via deflection of a laser off the back of the cantilever, which is monitored via a position-sensitive photodiode (PSPD). As the probe scans the surface and changes in the tip position result in changes in the laser deflection which is then fed to a feedback loop for control of tip position. Two additional commonly used AFM imaging modes are non-contact and intermittent contact (IC) mode. Hybrid or multimodal imaging modes, in which one or more other secondary techniques are combined with AFM imaging (discussed in **Section 5**), operate primarily with one or more of these three feedback modes. Contact

and IC mode are most relevant to the study of biological species, as both can operate in liquid or in air.

2.2 Contact mode. In contact mode, the tip is brought to the surface and the measured cantilever deflection is kept constant. Typical k_N values for AFM tips used in contact mode range from 0.01-90 N/m.[35] Some ways to achieve higher resolution in contact mode include operation in liquid, which eliminates attractive tip-sample capillary forces.[36] For instance, Lindsay and co-workers observed ~3 times greater lateral resolution and greater image contrast in topography images of λ bacteriophage DNA in liquid as compared to images acquired in air.[37] Other strategies to attain higher resolution in contact mode are use of a sharper tip[38] and decrease of the voltage setpoint after the tip snaps to contact on the initial approach.[39,40] Although high-resolution images are possible in contact mode,[36,41] other imaging modes, notably IC mode, often provide better resolution. Contact mode is less commonly used to image biological specimens due to a higher lateral force being applied to the sample via the tip during imaging, although for certain samples cellular topography images can be obtained without significant damage.[17, 42] For example, Goudonnet and co-workers were able to image the surface of living CV-1 kidney cells in contact mode with pN-range scanning forces and achieved lateral resolution better than 10 nm.[43]

2.3 IC mode. Intermittent contact mode, also known as alternating contact mode (AC mode) reduces the lateral forces applied on a sample.[44, 45] In IC mode the cantilever is oscillated at a user-defined amplitude and frequency close to f_o, such that the tip "taps" the surface while scanning. Intermittent contact mode is operated in the force regime known as 'intermittent contact', from which the mode derives its name.

Initially, IC mode was meant to operate in a non-contact regime where the tip experiences a net attractive force towards the sample. However, Zhang et al. demonstrated that greater resolution could be achieved if the oscillating tip was brought in closer contact with the surface and operated in a more repulsive-force regime.[46] Since the tip does not apply a constant force to the substrate, this mode is particularly useful for imaging soft, biological species as the tip will deform the sample less than in contact mode. In many experimental conditions, a phase shift (in oscillation) is observed when the tip interacts with the sample surface that is sensitive to viscoelasticity and tip-sample adhesion.[47] In many cases the signal from phase shifts result in marked and informative differences in contrast compared to topography. Additional strategies to achieve higher resolution in IC mode have been developed and include the use of a cantilever coated in magnetic material that is driven by an oscillating magnetic field.[48] Generally, strategies to reduce force applied by the tip to the sample will increase the resolution. One method would be to use a "soft" cantilever with a low quality or Q factor (measure of energy input to dissipation in a resonant system).[49]

2.4 AFM probes for cellular studies. Probe selection is an essential consideration for studying cellular and tissue systems with AFM. Both contact mode and IC mode probes are commonly fabricated from silicon and/or silicon nitride with well-established micromachining processes[50-53] and should be selected based on the imaging mode to be used and on the mechanical properties of the sample. **Figure 2** shows three probe configurations that can be used in contact mode imaging (**a**), IC mode imaging (**b**), and force spectroscopy (**c**) of biological samples. Force spectroscopy is an important mode of AFM used to probe mechanical properties of a

sample and will be discussed in detail in **Section 4**. In **Figure 2a** and **b**, *L, t,* and *W* correspond to length, width, and thickness of the cantilever, respectively. **Figures 2a** and **b** show schematic representations of the two most common cantilever shapes: a "diving-board" and a "V-shape". In addition to these common cantilever designs, modified cantilevers find utility in biological imaging. Carbon nanotubes, which have small tip diameters and are quite mechanically robust, have also been attached to the end of silicon tips to image high-aspect ratio features and to achieve superior lateral resolution.[54-59] In addition, Ag_2Ga nanowires can be grown onto the end of an AFM probe by to produce ultra-sharp tips, which have very unique properties, such as k_N values as low as 10^{-5} N/m.[60-62] The AFM probe in **Figure 2c** was fabricated by attachment of a 5 μm-diameter silica particle to a "V-shaped" (**Figure 2b**) probe with a micromanipulator.[63] The large contact area of this probe can result in less damage or less plastic deformation when force spectroscopy is performed on samples of low rigidity (*e.g.* epithelial cells).[63] However, an AFM probe with a large radius of curvature is a poor choice for high-resolution force mapping or for point measurements of molecules that are much smaller than the size of the probe.

Many types of AFM probes (*e.g.*, carbon nanotubes, gold coated silicon probes) can be readily functionalized with biomolecules or chemical functional groups.[64-66] For example, thiol-terminated hexasaccharides were attached to a gold-coated AFM probe to investigate interactions between oligoglucose saccharides and lectin concanavalin A.[65] In 2007 Chen et al. attached streptavidin-modified quantum dots via a disulfide linker to carbon nanotubes and delivered the molecules into living cells.[64] Upon entry to the cytosol, reduction of the disulfide bond liberated quantum dots from the cantilever.[64]

In some situations, the cell sample can even become the tip, as shown by Bowen et al., who utilized single *S. cerevisiae* (yeast) cells attached to tipless AFM cantilevers to measure adhesion forces.[67]

Probe material, shape and dimensions of the cantilever all affect the inherent physical attributes, such as f_o and k_N, of the probe. Material from which the probe is fabricated and the fabrication processes control the smallest tip size possible for an AFM probe. A list of parameters for silicon and silicon nitride probes, manufactured by MikroMasch®[35] and Olympus®,[68] respectively, are listed in **Figure 2d**. Cantilever *t* and *W* can fluctuate if coated with additional metallic layers (*e.g.*, Cr, Co, Au, Al, Pt), where each additional layer usually ranges from 10–60 nm in thickness.[35] Silicon nitride probes are often chosen for biological imaging as the k_N values of these probes tend to be smaller[68] which is essential for force spectroscopy studies on soft samples.[35, 68]

2.5 Substrate and environmental considerations for biological samples. The following section will review both general practices for preparing biological samples for AFM imaging and force spectroscopy and subsequently discuss more specific experimental considerations that are beneficial for the investigation of proteins, nucleic acids, viruses, cells and tissues.

The first consideration for biological sample imaging and force spectroscopy in general is the necessity of temperature, humidity and CO_2 control. For example, high AFM instrument operating temperatures cause a disruption in cell actin filament structure which leads to a decrease in cell elasticity as compared to cells probed in physiological conditions.[69] Through the use of a fluid cell and substrate heater, Li et al.

were able to study living breast cancer cells for several hours in culture medium at physiological temperature.[8]

For imaging discrete biomolecules, complexes or even single-molecules of proteins, nucleic acids or viral samples, deposition onto a surface for AFM imaging can be relatively simple. Protein, nucleic acid and virus imaging and force spectroscopy can be completed *in situ* in an appropriate buffer or *ex situ*. Exotic biomaterials, such as dolphin-shaped DNA origami[70] and self-assembled two-dimensional virus crystals[71] can be imaged with AFM by adsorbing a sample onto an appropriate surface. Mica, a crystal composed of silicate sheets,[72] is one of the most popular substrates for biological AFM imaging, as layers of mica can easily be cleaved with tape to create a clean, flat and chemically inert surface. In addition, mica has a very low root-mean-square (RMS) roughness (~0.05 nm),[73] which results in lower adhesive force between the tip and substrate.[74] Proteins, nucleic acids and viruses can also be immobilized on glass, but glass has a higher RMS value (~0.5 nm)[73] and must be chemically cleaned prior to sample deposition, whereas mica can quickly be cleaved to expose a clean substrate. Silicon, which has a low RMS value (<0.1 nm),[75] can also be used as an imaging substrate, but requires a more laborious cleaning procedure as compared to mica prior to AFM imaging. Highly oriented pyrolytic graphite (HOPG) usage is also widespread and layers can also be cleaved with tape to generate steps of clean, atomically smooth surfaces; yet, mica is often the preferred choice due to an inherent negative surface charge at physiological pH.[75] Protein, viral and nucleic acid samples prepared in buffer are commonly electrostatically adsorbed onto mica, HOPG or glass prior to imaging via incubation on the substrate for several minutes followed by an optional drying step

under a stream of nitrogen, depending on whether the sample is to be imaged in air or *in situ*. Optimizations of factors such as buffer composition, electrolyte composition, pH and sample concentration achieve optimal surface coverage for imaging is generally required. For example, Müller et al. found that purple membrane was better adsorbed to mica when the electrolyte concentration was sufficiently high and the EDL repulsion was less than the attractive vdW force.[76] In many situations additional surface functionalization may be required to encourage strong sample adsorption. For instance, in 2003 Shlyakhtenko et al. were only able to achieve time-lapse imaging of supercoiled DNA conformational changes, due to changes in the solution pH, after irreversible binding of DNA to a surface functionalized with 1-(3-aminopropyl)silatrane (APS).[77]

A significant fraction of AFM research related to disease requires cellular or tissues samples, which provide new challenges and complexities in sample preparation, dependent on the environment required. *Ex situ* cell samples are routinely imaged after chemical fixation and drying. Chemical fixation and drying methods have been developed to strengthen biological samples prior to imaging, similar to procedures employed to image cells with scanning electron microscopy (SEM). The main goal of chemical fixation is to preserve delicate features that may be structurally important to disease pathology, such as maintaining the physical integrity of heat shock proteins bound to stressed human umbilical venous endothelial cells.[78] Common fixative methods used to prepare samples include critical point drying[79] and incubation of the sample with dilute concentrations of glutaraldehyde,[80] formaldehyde,[81] or paraformaldehyde.[82] Francis et al. reported that the height integrity of Ishikawa cells (from differentiated human endometrial epithelial carcinomas[83]) fixed in solutions

containing 4% paraformaldehyde was found to be less than cells incubated in solutions with 3% glutaraldehyde, which highlights the importance of selection of fixative type.[84] Chemical fixation can also be useful for samples that tend to aggregate, such as viruses. Wang et al. found that mixing 2% glutaraldehyde with a suspension of recombinant adeno-associated virus serotype 2 decreased virus capsid compressions during imaging and reduced sample aggregation on mica.[85] An important step in chemical fixation is the drying step, which can be completed by critical point drying of the sample in ethanol, water, or an exotic organic solvent. In addition, samples can be dried in air by waiting for the solvent to completely evaporate, however surface tension from drying can damage some structures. For example, Francis et al. found that drying samples via evaporation in hexamethyldisilazane preserved finer Ishikawa cellular features compared to cells fixed with 3% glutaraldehyde.[84]

Cellular samples can also be imaged, and often are preferentially imaged, *in situ* (in culture medium or buffer) or *in vitro*, where fixatives are not used. Before a thorough discussion of sample preparation for *in situ* or *in vitro* cellular studies is undertaken, the cell exterior chemical environment, which often includes the extracellular matrix (ECM), will be considered. The ECM is a dynamic structure that provides a molecular scaffold and highly influences cell spreading, crawling, differentiation and adhesion;[86, 87] furthermore, the ECM may be of interest in live cell *in situ* or *in vitro* AFM experiments. The ECM is so significant to cell behavior that under identical serum conditions the phenotypic fate of native mesenchymal stem cells can be influenced solely by the elasticity of the matrix.[88] Mechanical properties of native ECM can be mimicked with careful attention to the surface chemistry and the mechanical nature of the underlying

substrate. A report from 2013 by Mata and co-workers, which describes the fabrication of a self-supported bioactive membrane, self-assembled from a positively charged multi-domain peptide and hyaluronic acid, elegantly illustrates the relationship between cell adhesion, spreading, substrate topography and surface chemistry.[89] Rat mesenchymal stem cells were cultured on the biomembrane and effects of the cell-adhesive amino acid sequence (arginine-glycine-aspartic acid-serine (RGDS)) in the membrane peptide, topographical membrane pattern, membrane thickness and polymer building block co-assembly on stem cell spreading and morphology were measured.[89] Another example of the importance of the ECM was demonstrated when the structure of fibronectin (an ECM glycoprotein), PC12 cell adhesion and cell differentiation were found to depend on surface chemistry and substrate topography.[90]

Atomic force microscopy is a very well-matched technique for *in situ* cellular studies as samples can be imaged in liquid with a high signal-to-noise ratio. For experiments in liquid, the role of both the substrate and liquid environment on sample adsorption must be carefully considered. Many of the surface types and chemical functionalizations reviewed for protein, virus and nucleic acid samples above can be applied to *in situ* AFM imaging of cells. For instance, the binding of outer membrane mitochondrial samples to 3-aminopropyltriethoxysilane (APTES)-modified mica was strong enough for successful AFM imaging even though the sample was placed in a liquid flow cell.[91] Although covalent bonding to a chemically-modified surface is often utilized,[92] physisorption of the sample-of-interest to the surface can be sufficient for immobilization because of the presence of hydrophobic interactions, the EDL, vdW, and electrostatic forces in a liquid environment.[74, 76].

Cells can be directly cultured onto the imaging substrate for *in vitro* AFM imaging and force spectroscopy. Imaging cells *in vitro* can be challenging, yet these are conditions more similar to the *in vivo* environment and experimentation in an *in vitro* environment may provide incredible insight into biochemically processes. Cellular function and structure are very sensitive to mechanical properties of the surface on which they are cultured.[93] Most biological cell culture in the last fifty years has been completed on polystyrene surfaces, which can readily be used in an AFM imaging experiment, but recent instances of cell culture on poly-dimethylsiloxane (PDMS) platforms has increased due to the material's low cost, ease of use and potential in microfabrication.[94] One finer nuance of cell culture on surfaces such as PDMS is the material's hydrophobicity/hydrophilicity. For example, functionalization with a polyethylene glycol-silane can render the surface appropriately hydrophilic for cell growth. Development of microscale systems for biological study has gained traction as these small platforms have led to an advanced understanding of cellular properties and the influence of the ECM on cell behavior, such as cell adhesion,[95] migration[96] and differentiation,[97] because features can be accurately controlled and systematically varied. In general, microscale structures are believed to shape general cell morphology, whereas nanoscale substrate variations are thought to effect sub-cellular features, such as filopodia.[98] Control of fine substrate features is not limited to PDMS and cells also can be grown on gels, such as poly-acrylamide[99] and poly-L-lysine/hyaluronic acid multilayers.[87] Microfabrication of substrates is especially complementary for use *in vitro* cellular studies related to disease. For instance, microhole structures have been shown to enhance osteogenesis *in vitro*[100] and guide retinal progenitor cell differentiation.[101]

Also, in 2008, Jinno et al. created a multilayer parylene C membrane stencil for patterning and co-culturing up to five different cell lines, which facilitated different cell population interactions during growth.[102]

The ultimate goal of native cell environment mimics is to create a hierarchical structure more reminiscent of *in vivo* three-dimensional tissue in which to study cell behavior. A number of recent attempts to recreate tissue scaffolds have been made that could be adapted to AFM studies of disease. For example, Mata and co-workers used a combination of electron-beam lithography, focused ion beam lithography, reactive-ion etching, photolithography and soft-lithography to create overlaid nanopatterns on microscale features.[103] In a 2013 report, Kolewe et al. introduced a new semi-automated layer-by-layer assembly method to fabricate planar poly-(glycerol sebacate) elastomeric sheets with pores that could be stacked to create tunable three-dimensional structural patterns, as shown in the schematic and SEM image in **Figure 3a** and **b**.[104] Alignment within the scaffold was tested by culturing mouse myoblast cells (C2C12) on the fabricated structure and was found to be high, as shown in the confocal fluorescence microscopy images in **Figure 3c** and **e**.[104] These types of three-dimensional scaffolds could be studied with AFM force spectroscopy to investigate elasticity of the abiotic scaffold itself or cultured cellular bundles and has applicability to biomedical implants.

Atomic force microscopy is broadly agreeable to the study of different tissue types, e.g. brain tissue,[105] bone,[106] teeth[107] and knee joint cartilage,[108] although sample preparation is highly dependent on the proposed system to be studied. Recently, AFM imaging of the dorsal striatum in a rodent brain was used to confirm the presence of

poly(amidoamine) dendrimers, a potential vehicle for drug delivery, at the blood brain barrier, which indicated an alteration in membrane permeability.[109] In this study, brain tissue was prepared immediately after rodent anesthetization and 4% paraformaldehyde perfusion, placed in 30% sucrose and shock frozen for cryopreservation.[109] Tissue sectioning by a cryostatic microtome was completed at -20 ˚C to produce 60 µm-thick slices which were stored in a mixture of phosphate buffered saline (PBS) and 0.05% sodium azide.[109] For experiments, brain slices were removed from the storage solution, air dried on glass slides and imaged in IC mode.[109] Atomic force microscopy imaging in air has also been employed to image human teeth dentin-enamel junctions (DEJ), which occur at the intersection of hard and soft tissue within the tooth.[110] These junctions were shown to be 2-3 µm wide and further AFM imaging of the DEJ could provide insight into the mechanical properties of the tooth for dental implants.[110] In this study, extracted human teeth were polished by hand with different diamond suspensions, down to 0.25 µm, to produce samples that were 1 mm thick.[110] In 2008, Stolz et al. reported early stage detection of structural and mechanical changes in human articular cartilage of aged non-osteoarthritic and osteoarthritic patients with *in situ* AFM force spectroscopy and imaging.[111] Here, articular cartilage was obtained from patients undergoing surgery and 2mm diameter-osteochondral plugs were acquired via a biopsy punch.[111] Prior to AFM imaging, plugs were immobilized on round Teflon disks with surgical glue and stored in ice cold PBS.[111]

2.6 Resolution and noise considerations. Stability, noise, and image resolution are important considerations for imaging small biological samples, such as proteins and viruses. Scanning probe microscopy resolution is a complex interplay

between many experimental parameters, from the probe material and dimensions to the type of sample to be imaged. Since the AFM probe is not an atomically sharp tip, long-range forces several nanometers away from the surface can influence image contrast. The influence of long-range vdW forces is an especially important resolution consideration for biological samples, which do not fit the two general sample criteria (hard and flat) for achieving high resolution.[24] However, despite sample limitations, 2D images of reconstituted sodium-driven rotors of bacterial ATP synthase in a lipid membrane have been recorded in contact mode in liquid with spatial resolution less than 1 nm, which amounts to resolution on the order of individual proteins.[112] In addition, molecules such as DNA are routinely imaged with vertical resolution less than 2 nm.[113] Topographic resolution can be instrument limited. For example, inherent properties of the piezoelectric material, such as hysteresis, can cause distortions in topographic images. In addition, the vertical range of piezopositioner may be physically limited (*e.g.*, limited to an extension of 10 μm), which could limit the height of samples that can be imaged with AFM. Scan rate can affect resolution as cells, proteins, viruses, etc. could become dislodged from the surface if the scan rate is too rapid in IC or contact mode; however, successful high-speed AFM (HS-AFM) imaging can achieve superior nanoscale resolution at high scan rates.[114] For instance, HS-AFM has been utilized to image the formation of supported lipid bilayers and 20 nm lipid nanotubes in real time by imaging at a scan rate of 975 milliseconds/frame.[115] In addition, lateral resolution is usually limited by *r*, although at larger scan sizes (>25 μm x 25 μm) pixel size can be the limiting factor. For example, the pixel size on a 50 μm x 50 μm scan, with 512 points/line, is 98 nm, which is much larger than the typical silicon tip radius (<10 nm).

Also, as discussed previously, resolution may be limited based on operation mode, as IC mode can generally give greater resolution than contact mode under similar experimental considerations. In IC mode, repulsive and attractive forces are balanced, which means that finer details can be imaged and resolved with minimized irreversible sample deformation.[116]

3. BIOANALYSIS VIA AFM IMAGING

3.1 Virus research. Viruses can readily be studied by AFM *in situ*[117, 118] or in air without the need for chemical fixation.[119] Common substrates used in virus research are mica, glass or HOPG. Oftentimes, AFM imaging is used to garner statistical size distributions of viruses[120] and/or to supplement other types of experimental data, such as mass spectra.[3, 121]

One of the most well-known viruses is human immunodeficiency virus (HIV). In a 2003 article by Kuznetsov et al., the first AFM images of HIV-infected human lymphocytes in culture were reported.[122] Interestingly, Kuznetsov et al. were able to visualize HIV-particles budding from lymphocytes.[122] Viruses were treated with mild detergents and inspected via topographical imaging,[122] which illustrates an advantage of imaging in liquid environments since *in situ* virus behavior be monitored at much shorter time scales than comparable techniques (e.g. electron microscopies).

A number of other viruses have been imaged with AFM. In 2003, the vaccinia virus, the basis of the smallpox vaccine, was imaged *in situ* with AFM for the first time and was the first well-resolved three dimensional rendition of the vaccinia virus capsid.[118] Another type of virus, the herpes simplex type 1 (HSV-1) virus, was recently

imaged in IC mode and some of the results of this study are shown in **Figure 4b-h**.[117] In **Figure 4a**, an electron micrograph shows several intact, protein envelope-free HSV-1 capsids.[117] Atomic force microscopy topography images are shown in **Figure 4b**, **c**, **e** and **f**. Here, individual capsomeres were distinguishable (**Figure 4c** and **e-h**) and the five and six nearest-neighbors capsomeres surrounding an individual can be seen (**Figure 4g** and **h**).[117] In addition, inspection of topographic images for irreversible capsid deformation demonstrated that viruses could withstand indentation forces of ~ 6 nN, which is very high.[117] Structural information like this recorded by AFM is important to develop a mechanistic understanding of the virus and for future drug development. The influenza virus was recently studied by Schaap et al. and AFM imaging in IC mode was shown to produce height measurements very similar to those made with cryoelectron microscopy, which suggests that in this particular experiment, capsid deformation by AFM was reversible.[123] In early 2013, AFM was used to irreversibly deform the picorna-like Triatoma virus[121], which is lethal to a species of tropical insect (*Triatoma infestans*)[124] and known to be the vector for Chagas disease.[125] Products of plastic deformation of the capsids by the AFM tip were imaged and primary products were found to be heterotrimeric pentons (5 copies) of the main proteins of structural assembly (VP1, VP2 and VP3), which helped elucidate a possible uncoating mechanism.[121]

3.2 Neuronal disease. The bulk of neuronal disease research with AFM has sought to elucidate the structure, subunits and mechanisms of the irreversible formation of single amyloids, which are protein fibrils linked to Alzheimer's[126] and Huntington's[127] disease. In 2010, a statistical AFM imaging study was undertaken to look at the

aggregation mechanisms of heated *β*-lactoglobulin fibrils, a well-characterized food product, to learn about amyloid fibril formation.[126] Amadcik et al. obtained high-resolution images of single *β*-lactoglobulin fibrils (**Figure 5a-d**) and compiled histograms of fibril contour length and height (**Figure 5e** and **f**).[126] Data collected suggested strong electrostatic interactions must exist, as heat-denatured fibrils were observed to form aggregates at a low pH (2).[126] The observations obtained by Amadcik et al. could potentially be applied to discover mechanisms of human amyloid aggregation. In another study, amyloid-*β* peptide (found in the plaque of sporadic Alzheimer's disease patients)-induced cellular toxicity of cultured fibroblasts was examined via high-resolution AFM imaging.[128] From a series of time-lapse AFM images, Zhu et al. found that amyloid-*β* peptide induces rapid cellular changes in fibroblasts, which includes the loss of cytoskeletal definition and cell-cell connections. Well-resolved IC mode AFM images of *in vitro,* self-aggregated amyloid-*β* peptides (1-42 residue) have also been collected by Arimon et al. in 2005.[129] This study provides insights into the mechanisms of amyloid-*β* peptide formation before aggregation and helps to confirm the existence of a nanometer-sized protofibril building block.[129]

Nerve cells can also be investigated via AFM. High-resolution images of myelinated and demyelinated axons of nerve tissue (the latter, a cause of multiple sclerosis[130]) were obtained in 2007 by Heredia et al.[17] Contact mode AFM images of these nerve cells were much better resolved that optical microscopy images. Also, topographic AFM imaging provided Heredia et al. the ability to distinguish demyelinated vs. myelinated nerve cells, which was essential as force spectroscopy mapping was later performed to investigate the mechanical differences between nerve cells with and

without myelination.[17] In 2009, different zones of live *Aplysia* growth cones were imaged in liquid by Xiong et al., which was a significant advance because little was known about the fine structure of growth cones under physiological conditions.[42] From AFM topography images of the P domain, T zone and C domain of neuronal growth cones, the height of each section was found to be approximately 183, 690 and 1322 nm, respectively, which interestingly was consistent with AFM measurements on fixed *Aplysia* growth cones.[42]

3.3 Cardiovascular disease. Atomic force microscopy is well-suited to study various components of the cardiovascular system. The structure of human erythrocytes has been investigated in contact mode and IC mode.[93] Previously, AFM has been used to image the crystal structure of annexin A5, an anticoagulant protein expressed by endothelial cells and placental thromboplasts.[131, 132] Specifically, in 2003, Rand et al. showed morphological evidence, via high-resolution AFM imaging, that antiphospholipid antibodies can disrupt annexin A5 binding to phospholipid membranes and cause an increase in thrombin generation, an important finding as increased vascular thrombosis can be a symptom of antiphospholipid syndrome and an indicator of endothelial injury.[131] Atomic force microscopy can also be used to study the effects of various conditions of living samples *in vitro*, such as aging of the cardiovascular system. Aging is known to be the cause of many diseases, including vascular diseases, and where the mechanism of individual cellular cytoskeleton changes can be difficult to study with fluorescence microscopy, AFM provides an alternative.[63] For example, Berdeyyva et al. imaged the cytoskeleton of young (less than 25 population doublings) and old (more than 50 population doublings) human epithelial cells after dissolving cellular proteins

with detergent.[63] To quantify these data, histograms of the distribution of fiber density and cytoskeleton volume for young and old cells were constructed from surface area and underlying projected areas obtained in topography images.[63] Overall conclusions from this study included thicker cytoskeletal structures, a greater apparent volume, and more randomly dispersed, thick globs (presumed to be polymerized proteins or lysosomes) on older cells than younger cells.[63]

More recent examples of AFM imaging in cardiovascular disease research include measurement of dynamic changes in real-time of angiotensin II type 1 blocker-stimulated mesangial cells[133] and studies of wild-type and desmin mutants to understand arrhythmogenic right ventricular cardiomyopathy[134]. Karagkiozaki et al. recently used AFM imaging to investigate platelet response of various biomaterials for potential use as stents.[135] More recently, AFM imaging has been better quantitated by mathematically defining analytical shape parameters when structural changes are observed.[136] A fascinating study was completed in 2013 by Du Plooy et al. to study the ultrafine structure of platelets from healthy human patients, tobacco smokers and stroke patients with AFM IC imaging in air.[80] Topography-height images, error images and high-resolution images of platelets from these three groups are shown in **Figure 6a**, **b** and **c**, respectively.[80] From these images, observation that stroke and smoker patient's platelets had more cytoskeletal rearrangement than the platelets of healthy patients was reported.[80] In addition, topography differences in these images supported results from other groups, namely that necrotic platelets are present in stroke patients[137] and that smoker's platelets have a change in membrane fluidity as compared to healthy individuals.[138] In another cardiovascular study last year, Oberleithner has shown a

physical interaction between blood and the vascular endothelium via AFM topography imaging.[139]

3.4 Cancer. One of the pathophysiological outcomes of cancer investigated with AFM is the softening of cancerous cells as compared to healthy ones.[8, 140, 141] Force spectroscopy and mapping are often performed to study cancer cells; however, this section will purely focus on imaging of cancerous systems, whereas mechanical property studies will be discussed in **Section 4**.

One of the advantages AFM offers over SEM or fluorescence microscopy is the ability to discern fine features on the cancerous cellular surfaces, such as the cytoskeleton[142] and the ECM.[143] Disruptions in the ECM can result in many diseases, including cancer; thus, various components of the ECM, such as collagen and elastins, are essential targets of study in disease research. In 2007, Friedrichs et al. demonstrated that when cells align on the ECM in a certain direction, significant deformation and re-organization of the individual collagen fibrils occurs.[144] Cellular polarization and directional traction was found to be the result of collagen pliability and high tensile strength of fibrils.[144] Atomic force microscopy can also be used to identify structural similarities between cancer cells that have many genetic differences. For instance, in 2005 a common actin-based structural feature, found to interact with components of the ECM, was identified on the surface of four different melanoma cell lines.[145]

Besides the ECM, other areas of interest in cancer research have been imaged and studied with AFM. For example, the stoichiometry of the 5-HT_3 receptor, a ligand-gated ion channel that is a therapeutic target for antiemetics in cancer therapy, was

resolved from AFM IC mode images in air.[146] Another study, completed in 2012, looked at the effects of glyphosate, an herbicide known to increase the risk of cancer, on human epidermal cells (HaCaT keratinocytes) with a high speed imaging technique (peak force tapping).[147] Heu et al. found that peak force tapping enabled chemically-induced cellular changes to be probed at near-physiological conditions of the entire cell.[147] Heu et al. concluded, from topography AFM images data, that glyphosate caused changes in cell integrity and the induced phenotype could be reversed through the application of the anti-oxidant, quercetin.[147] Surface roughness can be assessed in AFM images, which is useful for the determination of quantitative differences in cytoskeletal structure and membrane surfaces of cells with and without certain genes, such as the breast cancer metastasis suppressor 1 (BRMS-1) gene.[23] In the 2013 study by McEwen et al., AFM topography imaging revealed that BRMS-1 expression resulted in higher surface roughness of non-metastatic adenocarcinoma cells as compared to metastatic adenocarcinoma cells with no BRMS-1 expression.[23] These results indicate that cells with greater membrane surface roughness, as was found in cells expressing BRMS-1 as compared to cells with no suppressor expression, will adhere more strongly to a substrate, which could explain a part of the reason why there is a decreased metastatic potential in adenocarcinoma cells expressing BRMS-1.

4. MECHANICS OF CELLS AND TISSUES

Cells and tissues are complex structures, with organelles, cytosol, ECM components, etc., all of which contribute to overall mechanical properties. The ability to probe static and dynamic mechanics with AFM can help elucidate the underlying biochemical processes that govern cell function and morphology. Force curves are the

backbone of force spectroscopy and analysis. The restoring force (F_N) can also be thought of as the force compensating for the displacement of the tip by surface forces, where change in the tip position is represented by Δz. The restoring force is a property which can be exploited to investigate cellular elasticity and mechanics. From k_N, the Young's modulus (Y) can be calculated by:

$$k_N = \frac{Y*W*t^3}{4*L^3} \quad \textbf{(eq. 3)}^{148}$$

where L is the length of the cantilever, t is the cantilever thickness, and W is the cantilever width. The cantilever f_0 can be described by:

$$f_o = 0.162 * \frac{t}{L^2}\sqrt{\frac{Y}{\rho}} \quad \textbf{(eq. 4)}^{148}$$

where ρ is the mass density of the cantilever. Tip-sample forces can be plotted as a function of the extension of the piezoelectric positioner as the probe approaches a surface to extract relevant physical information, such as k_N. The force curve introduced in **Figure 1b** will be now be discussed in further detail. At a large z, the overall force felt by the tip is essentially zero and in this regime, cantilever deflection is zero (left-side of the plot shown in **Figure 1b**). As the tip is approached to the surface, atoms between the probe and the substrate begin to attract one another through vdW forces and these forces will cause the tip to abruptly snap into contact with the surface (noted as 'a' in **Figure 1b**). In this attractive region the AFM can be operated without touching the surface (*i.e.*, in non-contact mode). Once the tip is in contact with the surface (noted as region 'b' in **Figure 1b**), further advance of the tip results in an increased repulsive force. In ambient conditions, when the tip is retracted (noted as 'c' in **Figure 1b**), water or solvent inevitably present on both the surface and the tip generates an attractive capillary force (typically 10^{-8} N/m).[149] Once the tip "snaps off" the surface (noted as 'd'

in **Figure 1b**), forces which act on the tip are essentially zero again. The approach and retraction force curves shown in **Figure 1b** are meant to reflect the curve features in ambient conditions; however, the regions of the curves described above can also be applied to experiments performed in liquid to study the mechanical properties of living biological samples. In liquid environments, forces can be due to hydration, hydrophobic, and the electrical double layer forces, for instance.[150] One difference between force curves in liquid and ambient conditions is the shape difference in the retraction curve prior to the point that the tip snaps off the surface (noted as 'd' in **Figure 1b**). In addition, the slope of the linear region of the approach and retraction curves will be quite different for samples with different mechanical properties.

4.1 Force spectroscopy: approach curves. An approach curve (the first part of a force indentation cycle) is obtained when the tip-sample distance is decreased over an area of interest and cantilever deflection is monitored simultaneously.[149] For force curve interpretation, the k_N of the AFM cantilever should be calibrated experimentally. Most commonly, the thermal noise method is used to determine k_N before force curve acquisition.[151] Laser deflection from the cantilever measured experimentally can easily can be converted to force by Hooke's Law.[34] Typically, the movement of the piezo towards the sample covers 1-3 μm in the z-direction and will be performed at a frequency of 1-10 Hz (in IC mode).[14] A simple depiction of the approach curve into a soft, cellular sample is shown in **Figure 7**, in which cantilever deflection increases as the probe indents the cell.[152] Elastic properties (*i.e. Y*) of a biological sample can be measured through application of an appropriate model to the approach curve. Sometimes the Hertz model[153] is used to determine *Y*, yet assumptions of this model

can result in inconsistencies with approach curves acquired, for example on the edges of cells.[24] Finite element method simulations can be performed to more accurately describe deformation of the biological species, given the specific geometrical parameters and conditions of the experiment.[123] However, a number of useful models have been developed, which may benefit the reader.[123, 154-158] Viscoelasticity can also be measured with AFM approach curves and is a consequence of molecular rearrangements in a sample during indentation. A viscoelastic material possesses both viscous and elastic properties, meaning that the material can store and release mechanical energy dependent on the rate of deformation. Viscous and elastic forces that act on cantilever deflection can be slightly differentiated based on indentation time as generally short sub-second indentation times describe visoelastic behavior whereas long indentation times reveal the elastic response.[159] More detailed determination of mechanical transition points can be achieved through oscillation of the cantilever at different frequencies.[160] In addition, the probe loading rate may have an effect on the measured mechanical properties of a sample. For example, researchers recently quantitated the differences in mechanical properties of biomembranes and proteins based on the probe loading-rate.[161] These results could have consequences in force spectroscopy experiments performed on other biological samples if the findings can be generalized.

Stiffness measurements of cells, via force spectroscopy, have proven valuable in the study of disease states. Point-force spectroscopy is a well-established method to discriminate the mechanical differences of single cells after chemical treatment. For example, in 2007 Schäefer et al. used force spectroscopy to determine that ethanol-

treated nuclear pore complexes were stiffer than those not treated with ethanol, which may illustrate the damage increased alcohol consumption has on nuclear transport.[162] In addition, AFM has been used to track changes in leukemia cell stiffness from chemotherapy.[163] Atomic force microscopy can also be employed as a diagnostic tool for measurement of differences in the apparent Young's Modulus between benign and malignant human breast cancer cells.[8] Force spectroscopy has also found use in the discrimination of different cell phenotypes.[10, 13] Specifically, in 2012 Sulchek and co-workers measured a reduced stiffness (attributed to actin cytoskeleton remodeling) in highly invasive ovarian cancer cells as compared to a less invasive parent cell line.[10] Force curves can also be combined with other analyses, such as chemical assays, to link physical properties of species to biochemical pathways. For example, the success of immature HIV-type 1 entry was recently found to be directly related to capsid stiffness, which is regulated during maturation by the cytoplasmic tail of the transmembrane-anchored viral envelope protein.[11]

4.2 Force spectroscopy: retraction curves. The retraction part of a force curve is generated when the piezoelectric positioner retracts the tip from the surface and cantilever deflection is simultaneously measured. Many intra- and inter-molecular forces can be measured from the retraction region of a force-distance curve. For example, adhesion is a common intermolecular force probed via AFM and has been the target of investigation in human skin disease research,[164] cancer metastasis,[165] urinary tract microbial infections,[166] and fluoride treatment on teeth.[167] When the probe is retracted from the surface ('d' in **Figure 1b**), adsorbed proteins, cells, viruses, etc. exert an adhesive force on the tip and cause the probe to bend down towards the surface. This

adhesion force, or 'adhesive pull-off', is the force required to overcome tip-sample attachment as the probe is retracted and can be quantitated. In a retraction trace, a sharp peak is usually observed, which indicates the point of probe-sample detachment, and the adhesion force is the difference between this peak height and the force at large *z* distances (100-300 nm above the surface).

There have been several interesting examples of adhesion studies in the context of disease and a few will be reviewed here. In one study, adhesion force was measured to look at differences in heart mitochondrial swelling due to myocardial ischemia/reperfusion.[136] Lee et al. created histograms for each experimental group and found that between groups of rat models with induced myocardial ischemia/reperfusion and those with permanent ischemia, no statistically significant differences in adhesion force were noted. These results suggested that changes in the outer mitochondrial membrane occur regardless the degree of ischemia/reperfusion injury.[136] Squires and co-workers recently reported an AFM adhesion study of the effects of ketamine on proteins essential to healthy renal function, the results of which are shown in **Figure 8a**-**f**.[168] In this work, human epithelial cells of the proximal tubule were treated with different concentrations of ketamine and from biochemical methods were found to have variable protein expression. Force spectroscopy was employed to determine if these changes resulted in adhesive failures between two cells before biochemical cell function was compromised.[168] What is particularly intriguing about this study is that a single epithelial cell was attached to an AFM cantilever, brought into contact with a cellular cluster on the surface and then retracted to measure both the detachment energy/work of adhesion (gray area under curves in **Figure 8a**-**d**) and maximum unbinding force (force

value indicated by the red circles in **Figure 8a**-**d**).[168] Statistical analyses of these parameters, shown in **Figure 8e** and **f**, illustrate a dependence between ketamine concentration and increased cell detachment, which may explain the relationship between ketamine abuse and renal damage.[168]

Retraction regions of AFM force curves have also been used to study binding and rupture events between molecules or biological species tethered to the apex of AFM probes and their complement on the sample surface.[169-172] For example, the effect of aging on erythrocyte-fibrinogen binding has been investigated with force spectroscopy and the results showed that older erythrocytes bound less frequently with fibrinogen, but with no less force, due to an impairment in a specific fibrinogen-erythrocyte receptor interaction.[173] Intramolecular forces, such as protein unfolding, have been widely studied with AFM and can be an essential component to understanding the physical consequence of protein mutations. For example, a point-mutated titin, a protein involved in the elasticity of cardiac muscle, was found to have a compromised protein structure due to the decreased force required to unfold it as compared to the wild type titin.[18] Another example, reported by Tripathi et al, includes utilizing AFM probes functionalized with the pili adhesion protein, SpaC, to investigate via single-molecule force spectroscopy how the pili of probiotic, gram-positive *Lactobacillus rhamnosus* GG bacteria bind to hosts.[174] In this study researchers found that both homophilic (SpaC-SpaC) and heterophilic (SpaC-collagen or -mucin) connections have a similar adhesive strength, which suggest that the pili of *Lactobacillus rhamnosus* GG plays a very important role in the bacterial-host and bacterial-bacterial interactions within the intestinal environment.[174]

4.3 Force mapping. Since cell mechanical properties are often heterogeneous, a technique to map the distribution of force measurements, rather than a few point-by-point spectra, is essential develop a full picture of the cell.[175] Thus, to compare the relative differences in elasticity, adhesion, etc. force mapping has been developed.[176] For a detailed examination of force mapping, we refer the reader to an excellent review by Dufrêne et al.[177] A two-dimensional force map is generated by creating a two-dimensional 'force volume' of single force curves acquired over each imaging pixel.[24, 176, 177] From acquired force curves, elasticity, adhesion and deformation maps can be recorded and correlated to topography, with extremely high spatial resolution.[178] Three-dimensional AFM lateral force maps, where lateral forces between the tip and substrate are measured in both horizontal and vertical directions, have previously been completed in non-contact mode,[179, 180] but this technique is outside the scope of this review and will not be discussed. Additional imaging modes, such as friction force microscopy, can be generated simultaneously with topography, in contact mode, to investigate the interaction between chemical groups on the tip and the surface.[169] However, these types of images do not provide spatial information about specific mechanical properties of the sample.

Atomic force microscopy force mapping studies have been completed to elucidate mechanisms of bacterial-based respiratory infections,[181] to map the nanomechanical properties of amyloid fibrils from human *α*-synuclein proteins,[182] and to characterize the fuzzy coat on human Tau fibrils.[183] Differences in the elastic moduli of white and gray matter of rat cerebellum have been mapped with a larger tip (~ 20 μm radius) as well.[105] In 2012, Liu et al. were able to quantitate the difference in contraction

forces from living, beating cardiomyocytes derived from pluripotent stem cells of healthy subjects and those with dilated cardiomyopathy.[184]

Chemically-modified AFM probes can also be used to perform force mapping. For instance, hydrophobic regions on the surface of single mycobacterial cells in response to an anti-mycobacterial drug can be distinguished with chemically-modified probes.[185] Ligand-modified AFM probes are an excellent tool to map molecular recognition sites on biological surfaces. For example, Lama et al. performed single-molecule force mapping of gonadotropin-release hormone receptors on the surface of prostate cancer cells and the unbinding force between this receptor and analogue molecule (immobilized on the AFM probe).[186] However, the spatial resolution of unbinding events was poor in this study, despite high spatial resolution in topography images of the cell.[186] Another excellent single-molecule force mapping study with functionalized AFM probes was completed in 2010 by Alsteens et al. and for the first time demonstrated the utility of single-molecule AFM for the investigation of force-induced clustering of cell membrane receptors.[187] In this study, AFM probes were functionalized with antibodies specific to Als5p, an adhesin found in the fungus species *Candida albicans* that binds it to host tissues, to force-induce adhesion nanodomains within living yeast cells.[187] Single-molecule force mapping was employed to locate and quantify the adhesion force of the induced nanodomains. Through adhesion force mapping of the force-induced Als5p nanodomains, Alsteens et al. proposed that force-triggered Als5p proteins can interact and affect neighboring molecules to cause cell-wide activation of adhesion.[187]

5. HYBRID AFM TECHNIQUES

There are several excellent reviews and books that provide a more comprehensive assessment of a variety of hybrid AFM techniques.[188-192] The following section will review four classes of hybrid AFM techniques most relevant to the study of disease and single cell analysis: fluorescence microscopy-atomic force microscopy (FM-AFM), near-field scanning optical microscopy-atomic force microscopy (NSOM-AFM), scanning ion conductance microscopy-atomic force microscopy (SICM-AFM), and scanning electrochemical microscopy-atomic force microscopy (SECM-AFM)

5.1 Fluorescence microscopy-atomic force microscopy (FM-AFM). One reason for the widespread use of FM-AFM is the ease at which an optical microscope can be interfaced with an AFM (an example experimental set-up is shown in **Figure 9a**).[193] Also, AFM and fluorescence microscopy are highly complementary techniques and each provide unique advantages. For instance, AFM can be used to image objects smaller than the light diffraction limit and fluorescence microscopy can be used to detect fluorescent molecules below a cell surface. Hecht et al. observed changes in lung epithelial cell volume and height via AFM (see AFM topography image in **Figure 9b**), while fluorescence microscopy was employed concurrently as a method to confirm labeled-lamellar body fusion sites with the plasma membrane after chemical stimulation to induce exocytosis, despite the molecules being under the cell surface.[194] While data from AFM images and force spectroscopy are commonly used along with independent fluorescence microscopy data, for example to help explain variations in cellular elasticity

of prostate cancer cells,[195] this review will only focus on simultaneous fluorescence and AFM data acquisition experiments that have advanced disease research.

Combined FM-AFM has been useful to study a range of biological problems, such as inner ear cell development,[196] the three-dimensional landscape of fixed mast tumor cells,[20] and lipid membrane asymmetry.[197] Fluorescence microscopy-AFM encompasses a wide range of specific fluorescence techniques, such as confocal fluorescence,[21] total internal reflection fluorescence (TIRF)[198], and epifluorescence.[193, 199] In addition to combined AFM and fluorescence imaging, force spectroscopy can be extremely useful when performed in tandem with fluorescence excitation. For example, fluorescent-probe labeling of ions has been used to image chemical release events upon mechanical stimulation with the AFM probe.[200]

Several interesting examples of combined FM-AFM that have greatly added to knowledge for specific disease states have emerged in recent years. In 2009, AFM force spectroscopy and fluorescence microscopy were used together with a voltage-responsive fluorescent dye to determine the relationship between vascular endothelial cell stiffness and plasma membrane electrical potential.[193] Callies et al. discovered that sustained membrane depolarization is accompanied by a related increase in cell stiffness, while no relationship between these parameters was seen at small time scales.[193] Understanding the biological response to mechanical stress and/or stimulation is important for disease study. Using an FM-AFM, Kranz and co-workers reported a study in which a cell stretching device was incorporated into an FM-AFM instrument to observe the mechanical and structural changes in the cytokeratin network of fluorescently labeled squamous cell carcinoma cells.[201] High-speed AFM[114] has also

been incorporated with the fluorescence microscope.[202, 203] For instance, Fukuda et al. reported correlated AFM topography and TIRF microscopy images (shown in **Figure 9c**) where a fluorescently-labeled single chitinase A enzyme was observed moving along chitin microfibrils, at an imaging rate of 3 fps.[203]

Advantages and disadvantages exist for FM-AFM. As mentioned in the beginning of this section, AFM and fluorescence microscopy are very complimentary and quite easy to interface instrumentally. Also, fluorescence can provide some chemical specificity to AFM, which is a "chemically-blind" SPM tool. However, the use of this combined technique requires molecular labeling with fluorophores, which can be time-consuming, difficult and may alter molecule structure/function. Synchronization of image acquisition from both instruments is a major consideration in this technique. Determining and correlating AFM resolution with fluorescence image data can also be non-trivial, especially when observing a biological event over time. Often, the field of view will be different for the fluorescence and AFM images. For instance, from the two sets of images shown in **Figure 9c**, TIRF offers a wider field of view than the AFM.[203] Also, since most fluorescence imaging techniques are diffraction-limited, many sub-cellular events may be detectable via AFM, but not observable with sufficient spatial resolution with fluorescence microscopy alone to make correlating the images meaningful. Overall, however, FM-AFM is a robust, widely-used method to study disease states and perform single cell analysis that offers more chemical specificity than AFM alone.

5.2 Near-field scanning optical microscopy-atomic force microscopy (NSOM-AFM). Another powerful hybrid technique that can be utilized to study disease is NSOM-AFM, which was first suggested by Synge[204] in 1928 and experimentally

realized at visible wavelengths by Pohl[205] and Lewis[206] in 1984. Near-field optical techniques rely on the collection of short-range (a few nanometers from the surface of the illuminated object) evanescent waves. In itself, NSOM is a scanning probe technique, because it employs a sharp probe to scan a surface and either emits light or collects evanescent waves near the surface. The feedback mechanism is based on the strong distance-dependence of evanescent waves, which decay exponentially above the surface.[207] There are a multitude of NSOM operation modes, including transmission/illumination[208] and apertureless mode,[209] and also many styles of probes (*e.g.* an etched, metallic coated optical fiber[210]). Readers are referred to several reviews for more detailed information on NSOM.[207, 211-213] In this section, however, we will focus only on NSOM-AFM to perform imaging and spectroscopy on biological samples.

There are four main approaches in which AFM has been incorporated in NSOM. Schematics of these four methodologies are shown in **Figure 10a**-**d**. First, an optical fiber may be bent and etched to be used as a sharp probe controlled with AFM feedback and as the illumination or collector source (**Figure 10a**).[214] Second, a metal-coated AFM probe can be microfabricated to have an aperture at the tip apex, through which light is passed to the sample or collected (**Figure 10b**).[215, 216] Third, a commercially available, metallic AFM probe can be used as a sharp metallic object to provide localized field enhancements when externally illuminated. The third approach is also known as tip-enhanced NSOM (depicted in **Figure 10c**)[212, 217, 218] and can be used to perform simultaneous Raman spectroscopy.[219] The fourth method, called the tip-on-aperture approach, can be realized by placing a sharp, metallic tip (*i.e.* a coated optical

fiber or a microfabricated AFM probe) directly outside the aperture, so that field-enhancement occurs at the tip apex (**Figure 10d**).[220] Both tip-enhanced and tip-on-aperture NSOM offer greater resolution as compared to the other two NSOM-AFM approaches and have achieved lateral resolutions as low as 10-30 nm.[188]

Although NSOM-AFM is not as widely used as FM-AFM, a few groups have pursued research related to disease with this technique. For example, pioneering work was published by Muramatsu and co-workers in 2004 which described visualization of a specific gene sequence on a DNA molecule via detection of single-molecule fluorescence and topography imaging with NSOM-AFM.[221] Another study employed NSOM-AFM imaging to investigate the structure and fluorescence from labeled human lymphocyte chromosomes.[222] More recently, NSOM-AFM has been used to image fluorescently-labeled desmin protein fibrils, which are a part of the heart muscle cytoskeleton, with single-molecule resolution.[209]

Near-field scanning optical microscopy-AFM can serve as a technique to garner a wealth of chemical and spatial information from single cells. For example, an NSOM-AFM instrument can achieve greater fluorescence spatial resolution than most FM-AFM set-ups and can provide more chemical specificity than AFM alone. In addition, the feedback mechanism of NSOM and AFM can be decoupled in several operational modes and with certain tip configurations, which allows a wider range of sample types to be imaged. However, the complexity of instrumental operation, such as background light suppression, has most likely prevented NSOM-AFM from being more widely used in biological research. In addition, the emergence and wide-spread use of advanced fluorescence imaging techniques that can be easily interfaced with an AFM and offer

good spatial resolution, albeit not single molecule resolution, may discourage efforts to pursue NSOM-AFM experiments.

5.3 Scanning ion conductance microscopy-atomic force microscopy (AFM-SICM) Scanning ion conductance microscopy is an *in situ* SPM technique that relies on a nanopipette as the probe. Nanopipettes are pulled glass (*e.g.* borosilicate, quartz) capillaries fabricated with nanoscale orifice openings commonly below 50 nm, as shown in the SEM image in **Figure 11a**.[223-225] In SICM, the nanopipette is filled with electrolyte and immersed in a bath electrolyte solution. One reference electrode, such as a chloride-coated silver wire (*i.e.* an Ag/AgCl wire), is inserted into the nanopipette and the other is placed in the bath solution. If a potential bias is applied between the two electrodes, ion current can be measured. Feedback in SICM relies on the distance-dependence of the ion current signal close to and far from the surface. One advantage of SICM is that the nanopipette probe does not come into physical contact with the sample and is thus an excellent SPM technique to measure living biological samples.[226] One of the first combined AFM-nanopipette experiments was completed by Hörber et al. in 1995 in which *Xenopus* oocytes were investigated via a patch-clamp technique.[227] These experiments were significant because the surface topology of the membrane was imaged, via the AFM, simultaneously with electrical recordings via nanopipettes. Also, Hörber et al. were able to investigate the extent of cytoskeletal changes due to the pressure exerted by the patch pipette, which was statically held on the membrane during imaging with the AFM probe.[227] However, in these experiments, the pipette and AFM probe were separate entities and thus completely decoupled.

Another mode of SICM-AFM makes use of the nanopipette as both the force and ion conductance sensor. For instance, a nanopipette suitable for SICM can be bent to more closely resemble an AFM probe (**Figure 11b**).[25, 228, 229] Proksch et al. were able to achieve SPM feedback using laser-deflection on this type of bent pipette probe, which was mounted into a commercial AFM microscope, similar to contact or IC mode AFM.[228] In initial experiments, a hydrophilic porous polymer membrane was imaged and ion conductance through the membrane was measured simultaneously.[228] Although this mode of operation appeared promising and this probe type was commercialized,[230] nanopipette-based AFM probes for combined imaging were not widely adopted. One avenue where these types of probes may find use is through controlled delivery of chemical species, such as fluorescently-labeled molecules.[231]

There are a number of benefits of SICM-AFM for disease research. Scanning ion conductance microscopy-atomic force microscopy can be advantageous as compared to SICM because ion current and probe feedback are decoupled, which may afford higher resolution images. In addition, ion current measurements add an auxiliary signal not previously accessible in AFM. However, this technique may be considered somewhat niche and has not been widely applied. For example, since the first report of SICM-AFM in 1996,[228] less than 20 papers have been published which describe an SICM-AFM instrument configuration. The difficulty of probe fabrication, in the case of a bent nanopipette/AFM probe, may be considered a small drawback. Also, SICM has been much more widely adopted and commercialized in the last decade; thus, labs can perform separate AFM and SICM experiments in-house and simultaneous topography, ion current, etc. images may not be necessary. Amazingly, nanopipettes can now be

used alone to acquire topographic and force data simultaneously to create stiffness maps of cells due to an increased understanding of hydrodynamic liquid flow through the probe.[232] Indeed, force measurements with SICM in general seem to be gaining popularity within the last few years[232] and compete well with AFM techniques.

5.4 Scanning electrochemical microscopy-atomic force microscopy (SECM-AFM). Scanning electrochemical microscopy is another type of SPM tool that makes use of conductive ultramicroelectrodes (UMEs, *i.e.* an electrode with dimensions < 25 μm)[233] to spatially map electrochemical redox processes through the detection of Faradaic current in liquid.[234] Scanning electrochemical microscopy is based on a conventional three or four electrode system, where one or two working electrodes, a reference electrode and a counter electrode are present. Several operating modes exist, such as positive feedback[235] and generation-collection mode,[236] for which various feedback mechanisms and experimental configurations are employed. For a more comprehensive review of SECM, the reader is referred to several texts.[237-244]

An SECM-AFM instrument is capable of operation in AFM contact[245] and IC mode[246, 247]. In either operation, faradaic redox current is collected from a small electrode at or near the AFM tip apex while topography is collected simultaneously. Most notably, the electrochemical signal and probe feedback are decoupled.[245] The first SECM-AFM experiment was completed by Macpherson et al. in 1996, who examined probe-induced electrochemical dissolution of ferrocyanide crystals.[248] Since AFM feedback is based on laser deflection, faradaic current can be measured independent of probe position. In most SECM-AFM experiments, the use of a redox probe, such as ferrocene methanol, or ferricyanide, is used to measure Faradaic current from a redox

process. The role of the AFM probe in SECM-AFM operation is analogous to the working electrode in a conventional three-electrode system. An example SECM-AFM experiment is shown in **Figure 12a**, top, which depicts diffusion of $Ru(NH_3)_6^{3+}$ (a model redox probe) through a porous poly-imide membrane from the bottom chamber of a diffusion cell to the top chamber.[249] Here, the AFM probe, which is insulated with parylene C, scans the surface while simultaneously recording the reduction current of the redox mediator to produce correlated topography (**Figure 12a**, lower left) and current (**Figure 12a,** lower right) maps. The substrate can also serve as a second working electrode (four-electrode SECM-AFM).[246]

Fabrication of SECM-AFM probes encompasses a small sub-field of SECM-AFM, as the geometry, material and electrical isolation of the UME in an AFM probe is critical to experimental success. Probes utilized in SECM-AFM can have one dimension smaller than 100 nm and are often referred to as nanoelectrodes.[250] In SECM-AFM, a conductive AFM probe is coated with a insulative layer to create an ultramicroelectrode at the tip apex[245] or at another well-defined region of the probe.[246] An example SECM-AFM probe, insulated in parylene C, is shown in the SEM image in **Figure 13b**, in which a gold frame UME has been exposed and recessed from a re-shaped silicon tip via focused ion beam (FIB) milling.[246] Probes insulated with electrophoretic paint,[245,251] silicon nitride,[252-256] silicon oxide,[257] polyfluoroethane,[258] photoresist[259] and parylene[249, 260-263] have been successfully explored. Typically, gold[246] and platinum[245, 264] probes are used as the conductive material in SECM-AFM tip fabrication; however, carbon nanotube,[265] boron-doped diamond[266] and platinum carbon composite[267] SECM-AFM probes have been realized. In all instances, the AFM probe must be electrically

insulated and a well-defined electrode area must be achieved. Previously, the electro-active area of the probe has been defined and exposed via FIB milling,[252, 255, 258, 262, 263, 266, 268, 269] electron beam lithography,[253] heat recession of an electrodeposition paint,[245, 251] UV illumination[259] and electrical arcing.[251] Wafer-level batch fabrication of silicon nitride SECM-AFM probes has been accomplished as well.[257, 270] In addition, redox-active molecules can be covalently attached to an AFM probe via poly(ethylene glycol) (PEG) as a method to probe nanoscale sites.[271-274]

A number of studies have been completed in disease research with SECM-AFM. Experiments imaging the diffusion of redox molecules through abiotic porous membranes[245, 249] demonstrate the future applicability of this technique for probing cellular release of electroactive molecules, such as dopamine. In one instance, Mizaikoff and co-workers employed SECM-AFM to measure glucose oxidase enzyme activity in IC mode.[246] In a study by Demaille and co-workers, the conformation and motional dynamics of single- and double-stranded DNA were probed via SECM-AFM.[275] The data indicated that DNA hybridization can be detected at the low limit of ~200 molecules with SECM-AFM.[275] Other experimental results by Agnes et al. demonstrate the incredible utility of probes with redox-PEG linkers for probing proteins that are not electroactive, which could have a significant impact in disease research.[272] The instrument schematic used in this study is shown in **Figure 13c** and depicts electron transfer from a conductive, biased substrate through a target protein, which is bound to a redox-labeled mouse immunoglobulin (IgG) antibody, to the electroactive area of the probe.[272] Topographical and electrochemical surface distribution of mouse IgG antigens were mapped on a surface with resolution of ~100 nm, which indicates that this

technique can be used to distinguish labeled target proteins from similarly-sized items.[272]

Electrochemical results from experiments that utilized intrinsic probes can be difficult to interpret since the electrode size can change as the probe scans the surface. Extrinsic tips allow for simultaneous current and topography measurement, but usually require complex instrumental techniques for fabrication, such as a FIB milling, electron beam lithography and standard lithographic patterning. Fabrication of either probe type is labor intensive and is the limiting factor for SECM-AFM popularity. In addition, most SECM-AFM experiments reported have been done under idealized conditions (*e.g.*, using a porous membrane) and have not be used to study living cells. Also, the accelerated usage of a SECM-SICM, which has been used to image live cells[276] and may prove less damaging for non-contact imaging of biological species as compared to SECM-AFM, also indicates a decline in necessity for SECM-AFM experiments in disease research.

CONCLUSIONS AND FUTURE PROSPECTS

Although diagnostic care will always be essential to preventing and managing disease, the importance of understanding the basic cellular mechanisms which underlie these diseases cannot be understated. Atomic force microscopy is a suburb technique to study micro- and nanoscale biochemical and mechanical processes on living cellular systems relating to diseases. Often, model cell lines are cultured to study a host-pathogen relationship, which can either be imaged or probed in real-time with this technique. Most importantly, AFM is not merely an imaging technique, but can be used to spatially probe the mechanical properties different biological species in various disease states. To add chemical specificity to the technique, the end of the AFM probe

can be functionalized with biomolecules to study intra- and intermolecular forces. Perhaps one of the greatest advantages of AFM is its accessibility to inexperienced users due to straight-forward operating software and commercially available instruments. Another superior advantage is that the AFM can readily be interfaced with other types of microscopies and spectroscopies to acquire simultaneous data sets. In fact, AFM is so seamlessly merged with other microscopies that tri-modal NSOM-AFM-SECM imaging can be performed with a single probe![277]

Although AFM has enjoyed dominance over many other types of SPMs and light microscopies for the last 30 years due to high spatial resolution and ability to probe the mechanical properties of soft biological samples, the gap between this technique and others are closing. Groups now use alternative scanned probes, as well as super-resolution optical microscopy, for biological imaging, as the fine features on cellular surfaces can be easily imaged. In addition, SICM is now being used as a local method to probe forces in biological cells. There is some evidence that in certain conditions, AFM may actually underestimate cell heights and lateral forces during imaging, even in IC mode, are still an issue.[278] However, the wide-spread use of AFM beyond purely academic setting is one indicator of its permanent place in the library of commonly used analytical techniques for single cell analysis and disease research.

ACKNOWLEDGEMENTS

We would like to acknowledge funding from the Research Corporation for Scientific Advancement and the National Science Foundation (NSF) (CHE-0847642) for funding. In addition, Anna Weber and Elizabeth Yuill are thanked for helpful comments and edits to this manuscript.

REFERENCES

1. B. Vileno, M. Lekka, A. Sienkiewicz, S. Jeney, G. Stoessel, J. Lekki, L. Forro and Z. Stachura, *Environ. Sci. Technol.*, 2007, **41**, 5149-5153.

2. A. Reich, M. Meurer, A. Viehweg and D. J. Müller, *Photochem. Photobiol.*, 2009, **85**, 1-7.

3. C. Uetrecht, C. Versluis, N. R. Watts, W. H. Roos, G. J. L. Wuite, P. T. Wingfield, A. C. Steven and A. J. R. Heck, *Proc. Natl. Acad. Sci. U.S.A.*, 2008, **105**, 9216-9220.

4. A. Kuypers, P. M. W. Willems, M. J. Vanderschans, P. C. M. Linssen, H. M. C. Wessels, C. Debruijn, F. M. Everaerts and E. Mensink, *J. Chromatogr. B*, 1993, **621**, 149-156.

5. K. Leonhardt, A. Avdic, A. Lugstein, I. Pobelov, T. Wandlowski, B. Gollas and G. Denuault, *Electrochem. Commun.*, 2013, **27**, 29-33.

6. R. Zenobi, *Science*, 2013, **342**, 1243259.

7. G. Y. H. Lee and C. T. Lim, *Trends Biotechnol.*, 2007, **25**, 111-118.

8. Q. S. Li, G. Y. H. Lee, C. N. Ong and C. T. Lim, *Biochem. Biophys. Res. Commun.*, 2008, **374**, 609-613.

9. A. L. J. Olsson, N. Arun, J. S. Kanger, H. J. Busscher, I. E. Ivanov, T. A. Camesano, Y. Chen, D. Johannsmann, H. C. van der Mei and P. K. Sharma, *Soft Matter*, 2012, **8**, 9870-9876.

10. W. Xu, R. Mezencev, B. Kim, L. Wang, J. McDonald and T. Sulchek, *PLoS One*, 2012, **7**, e46609.

11. H.-B. Pang, L. Hevroni, N. Kol, D. M. Eckert, M. Tsvitov, M. S. Kay and I. Rousso, *Retrovirology*, 2013, **10**.

12. C. Braunsmann, C. M. Hammer, J. Rheinlaender, F. E. Kruse, T. E. Schäeffer and U. Schlöetzer-Schrehardt, *Invest. Ophthalmol. Vis. Sci.*, 2012, **53**, 2960-2967.

13. E. U. Azeloglu, J. Bhattacharya and K. D. Costa, *J. Appl. Physiol.*, 2008, **105**, 652-661.

14. K. D. Costa, *Dis. Markers*, 2004, **19**, 139-154.

15. G. Binnig, C. F. Quate and C. Gerber, *Phys. Rev. Lett.*, 1986, **56**, 930-933.

16. R. Krautbauer, M. Rief and H. E. Gaub, *Nano Lett.*, 2003, **3**, 493-496.

17. A. Heredia, C. C. Bui, U. Suter, P. Young and T. E. Schäeffer, *Neuroimage*, 2007, **37**, 1218-1226.

18. B. R. Anderson, J. Bogomolovas, S. Labeit and H. Granzier, *J. Biol. Chem.*, 2013, **288**, 5303-5315.

19. B. Drake, C. B. Prater, A. L. Weisenhorn, S. A. C. Gould, T. R. Albrecht, C. F. Quate, D. S. Cannell, H. G. Hansma and P. K. Hansma, *Science*, 1989, **243**, 1586-1589.

20. D. J. Frankel, J. R. Pfeiffer, Z. Surviladze, A. E. Johnson, J. M. Oliver, B. S. Wilson and A. R. Burns, *Biophys. J.*, 2006, **90**, 2404-2413.

21. R. Kassies, K. O. Van der Werf, A. Lenferink, C. N. Hunter, J. D. Olsen, V. Subramaniam and C. Otto, *J. Microsc.*, 2005, **217**, 109-116.

22. O. S. Ovchinnikova, K. Kjoller, G. B. Hurst, D. A. Pelletier and G. J. Van Berkel, *Anal. Chem.*, 2014, **86**, 1083-1090.

23. G. D. McEwen, Y. Wu, M. Tang, X. Qi, Z. Xiao, S. M. Baker, T. Yu, T. A. Gilbertson, D. B. DeWald and A. Zhou, *Analyst*, 2013, **138**, 787-797.

24. A. Alessandrini and P. Facci, *Meas. Sci. Technol.*, 2005, **16**, R65-R92.

25. R. Lal and R. Proksch, *Int. J. Imag. Syst. Tech.*, 1997, **8**, 293-300.

26. R. M. Henderson and H. Oberleithner, *Am. J. Physiol.-Renal*, 2000, **278**, F689-F701.

27. Z. Deng, V. Lulevich, F.-t. Liu and G.-y. Liu, *J. Phys. Chem. B*, 2010, **114**, 5971-5982.

28. N. E. Kurland, Z. Drira and V. K. Yadavalli, *Micron*, 2012, **43**, 116-128.

29. X. T. Zheng and C. M. Li, *Chem. Soc. Rev.*, 2012, **41**, 2061-2071.

30. Y. F. Dufrêne and A. E. Pelling, *Nanoscale*, 2013, **5**, 4094-4104.

31. L. W. Francis, P. D. Lewis, C. J. Wright and R. S. Conlan, *Biol. Cell*, 2010, **102**, 133-143.

32. J. Israelachvili, *Intermolecular and Surface Forces*, 2nd edn., Academic press, London, UK, 1991.

33. A. J. Bard and L. R. Faulkner, *Electrochemical Methods: Fundamentals and Applications*, 2nd edn., John Wiley & Sons, Hoboken, NJ, 2001.

34. K. Kolasinski, *Surface Science: Foundations of Catalysis and Nanoscience*, 2nd edn., John Wiley & Sons, LTD., West Sussex, UK, 2008.

35. SPM Probes and Test Structures: MikroMasch Product Catalog. http://www.spmtips.com/ (accessed Nov 14, 2013).

36. F. Ohnesorge and G. Binnig, *Science*, 1993, **260**, 1451-1456.

37. Y. Lyubchenko, L. Shlyakhtenko, R. Harrington, P. Oden and S. Lindsay, *Proc. Natl. Acad. Sci. U.S.A.*, 1993, **90**, 2137-2140.

38. S. P. Jarvis, S. I. Yamamoto, H. Yamada, H. Tokumoto and J. B. Pethica, *Appl. Phys. Lett.*, 1997, **70**, 2238-2240.

39. F. J. Giessibl, *Phys. Rev. B.*, 1992, **45**, 13815-13818.

40. F. J. Giessibl and G. Binnig, *Ultramicroscopy*, 1992, **42**, 281-289.

41. M. R. Jarvis, R. Perez and M. C. Payne, *Phys. Rev. Lett.*, 2001, **86**, 1287-1290.

42. Y. Xiong, A. C. Lee, D. M. Suter and G. U. Lee, *Biophys. J.*, 2009, **96**, 5060-5072.

43. C. Le Grimellec, E. Lesniewska, M.-C. Giocondi, E. Finot, V. Vié and J.-P. Goudonnet, *Biophys. J.*, 1998, **75**, 695-703.

44. J. Berg and G. A. D. Briggs, *Phys. Rev. B.*, 1997, **55**, 14899-14908.

45. T. M. H. Wong and P. Descouts, *J. Microsc.*, 1995, **178**, 7-13.

46. Q. Zhong, D. Inniss, K. Kjoller and V. B. Elings, *Surf. Sci.*, 1993, **290**, L688-L692.

47. H. G. Hansma, K. J. Kim, D. E. Laney, R. A. Garcia, M. Argaman, M. J. Allen and S. M. Parsons, *J. Struct. Biol.*, 1997, **119**, 99-108.

48. G. L. Ge, D. Han, D. Y. Lin, W. G. Chu, Y. X. Sun, L. Jiang, W. Y. Ma and C. Wang, *Ultramicroscopy*, 2007, **107**, 299-307.

49. J. K. H. Hörber and M. J. Miles, *Science*, 2003, **302**, 1002-1005.

50. S. Akamine, R. C. Barrett and C. F. Quate, *Appl. Phys. Lett.*, 1990, **57**, 316-318.

51. A. Folch, M. S. Wrighton and M. A. Schmidt, *J. Microelectromech. Syst.*, 1997, **6**, 303-306.

52. O. Wolter, T. Bayer and J. Greschner, *J. Vac. Sci. Technol., B*, 1991, **9**, 1353-1357.

53. T. R. Albrecht, S. Akamine, T. E. Carver and C. F. Quate, *J. Vac. Sci. Technol., A*, 1990, **8**, 3386-3396.

54. C. L. Cheung, J. H. Hafner and C. M. Lieber, *Proc. Natl. Acad. Sci. U.S.A.*, 2000, **97**, 3809-3813.

55. H. J. Dai, J. H. Hafner, A. G. Rinzler, D. T. Colbert and R. E. Smalley, *Nature*, 1996, **384**, 147-150.

56. J. H. Hafner, C. L. Cheung and C. M. Lieber, *J. Am. Chem. Soc.*, 1999, **121**, 9750-9751.

57. J. H. Hafner, C. L. Cheung and C. M. Lieber, *Nature*, 1999, **398**, 761-762.

58. H. Nishjima and S. Kamo, *Appl. Phys. Lett.*, 1999, **74**, 4061-4063.

59. A. T. Woolley, C. Guillemette, C. Li Cheung, D. E. Housman and C. M. Lieber, *Nat. Biotechnol.*, 2000, **18**, 760-763.

60. M. M. Yazdanpanah, S. A. Harfenist, A. Safir and R. W. Cohn, *J. Appl. Phys.*, 2005, **98**.

61. V. V. Dobrokhotov, M. M. Yazdanpanah, S. Pabba, A. Safir and R. W. Cohn, *Nanotechnology*, 2008, **19**.

62. L. B. Biedermann, R. C. Tung, A. Raman, R. G. Reifenberger, M. M. Yazdanpanah and R. W. Cohn, *Nanotechnology*, 2010, **21**.

63. T. K. Berdyyeva, C. D. Woodworth and I. Sokolov, *Phys. Med. Biol.*, 2005, **50**, 81-92.

64. X. Chen, A. Kis, A. Zettl and C. R. Bertozzi, *Proc. Natl. Acad. Sci. U.S.A.*, 2007, **104**, 8218-8222.

65. A. Touhami, B. Hoffmann, A. Vasella, F. A. Denis and Y. F. Dufrêne, *Langmuir*, 2003, **19**, 1745-1751.

66. S. S. Wong, E. Joselevich, A. T. Woolley, C. L. Cheung and C. M. Lieber, *Nature*, 1998, **394**, 52-55.

67. W. R. Bowen, R. W. Lovitt and C. J. Wright, *J. Colloid Interface Sci.*, 2001, **237**, 54-61.

68. Silicon Nitride Cantilevers. http://probe.olympus-global.com/en/product/siliconnitride.cfm (accessed Nov 14, 2013).

69. Y.-W. Chiou, H.-K. Lin, M.-J. Tang, H.-H. Lin and M.-L. Yeh, *PLoS One*, 2013, **8**, e77384.

70. E. S. Andersen, M. Dong, M. M. Nielsen, K. Jahn, A. Lind-Thomsen, W. Mamdouh, K. V. Gothelf, F. Besenbacher and J. Kjems, *ACS Nano*, 2008, **2**, 1213-1218.

71. J. Sun, C. DuFort, M.-C. Daniel, A. Murali, C. Chen, K. Gopinath, B. Stein, M. De, V. M. Rotello, A. Holzenburg, C. C. Kao and B. Dragnea, *Proc. Natl. Acad. Sci. U.S.A.*, 2007, **104**, 1354-1359.

72. S. W. Bailey, *Rev. Mineral.*, 1984, **13**, 13-60.

73. D. N. Fronczek, C. Quammen, H. Wang, C. Kisker, R. Superfine, R. Taylor, D. A. Erie and I. Tessmer, *Ultramicroscopy*, 2011, **111**, 350-355.

74. H. J. Butt, B. Cappella and M. Kappl, *Surf. Sci. Rep.*, 2005, **59**, 1-152.

75. C. N. Buechner and I. Tessmer, *J. Mol. Recognit.*, 2013, **26**, 605-617.

76. D. J. Müller, M. Amrein and A. Engel, *J. Struct. Biol.*, 1997, **119**, 172-188.

77. L. S. Shlyakhtenko, A. A. Gall, A. Filonov, Z. Cerovac, A. Lushnikov and Y. L. Lyubchenko, *Ultramicroscopy*, 2003, **97**, 279-287.

78. G. Pfister, C. M. Stroh, H. Perschinka, M. Kind, M. Knoflach, P. Hinterdorfer and G. Wick, *J. Cell Sci.*, 2005, **118**, 1587-1594.

79. L. Chang, T. Kious, M. Yorgancioglu, D. Keller and J. Pfeiffer, *Biophys. J.*, 1993, **64**, 1282-1286.

80. J. N. Du Plooy, A. Buys, W. Duim and E. Pretorius, *PLoS One*, 2013, **8**, e69774.

81. G. Weissmüller, J. Garcia-Abreu, P. M. Bisch, V. M. Neto and L. A. Cavalcante, *Neurosci. Res.*, 2000, **38**, 217-220.

82. M. Moloney, L. McDonnell and H. O'Shea, *Ultramicroscopy*, 2004, **100**, 153-161.

83. M. Nishida, K. Kasahara, M. Kaneko and H. Iwasaki, *Acta Obstet. Gynaecol. Jpn.*, 1985, **37**, 1103-1111.

84. L. W. Francis, D. Gonzalez, T. Ryder, K. Baer, M. Rees, J. O. White, R. S. Conlan and C. J. Wright, *J. Microsc.*, 2010, **240**, 111-121.

85. P. Wang, X. Wang, H. Yang and J. Lue, *Surf. Rev. Lett.*, 2008, **15**, 595-598.

86. A. J. Engler, M. A. Griffin, S. Sen, C. G. Bonnetnann, H. L. Sweeney and D. E. Discher, *J. Cell Biol.*, 2004, **166**, 877-887.

87. A. J. Engler, L. Richert, J. Y. Wong, C. Picart and D. E. Discher, *Surf. Sci.*, 2004, **570**, 142-154.

88. A. J. Engler, S. Sen, H. L. Sweeney and D. E. Discher, *Cell*, 2006, **126**, 677-689.

89. A. C. Mendes, K. H. Smith, E. Tejeda-Montes, E. Engel, R. L. Reis, H. S. Azevedo and A. Mata, *Adv. Funct. Mater.*, 2013, **23**, 430-438.

90. S. S. Jedlicka, J. L. McKenzie, S. J. Leavesley, K. M. Little, T. J. Webster, J. P. Robinson, D. E. Nivens and J. L. Rickus, *J. Mater. Chem.*, 2006, **16**, 3221-3230.

91. Y. Tian, J. Li, M. Cai, W. Zhao, H. Xu, Y. Liu and H. Wang, *RSC Advances*, 2013, **3**, 708-712.

92. S. Karrasch, M. Dolder, F. Schabert, J. Ramsden and A. Engel, *Biophys. J.*, 1993, **65**, 2437-2446.

93. I. Dulinska, M. Targosz, W. Strojny, M. Lekka, P. Czuba, W. Balwierz and M. Szymonski, *J. Biochem. Bioph. Methods*, 2006, **66**, 1-11.

94. E. Berthier, E. W. K. Young and D. Beebe, *Lab Chip*, 2012, **12**, 1224-1237.

95. M. Arnold, M. Schwieder, J. Bluemmel, E. A. Cavalcanti-Adam, M. Lopez-Garcia, H. Kessler, B. Geiger and J. P. Spatz, *Soft Matter*, 2009, **5**, 72-77.

96. S. Raghavan, R. A. Desai, Y. Kwon, M. Mrksich and C. S. Chen, *Langmuir*, 2010, **26**, 17733-17738.

97. R. Peng, X. Yao and J. Ding, *Biomaterials*, 2011, **32**, 8048-8057.

98. M. M. Stevens and J. H. George, *Science*, 2005, **310**, 1135-1138.

99. R. J. Pelham and Y. L. Wang, *Proc. Natl. Acad. Sci. U.S.A.*, 1997, **94**, 13661-13665.

100. A. Wilkinson, R. N. Hewitt, L. E. McNamara, D. McCloy, R. M. D. Meek and M. J. Dalby, *Acta Biomater.*, 2011, **7**, 2919-2925.

101. M. R. Steedman, S. L. Tao, H. Klassen and T. A. Desai, *Biomed. Microdevices*, 2010, **12**, 363-369.

102. S. Jinno, H.-C. Moeller, C.-L. Chen, B. Rajalingam, B. G. Chung, M. R. Dokmeci and A. Khademhosseini, *Journal of Biomedical Materials Research Part A*, 2008, **86A**, 278-288.

103. M. J. Lopez-Bosque, E. Tejeda-Montes, M. Cazorla, J. Linacero, Y. Atienza, K. H. Smith, A. Llado, J. Colombelli, E. Engel and A. Mata, *Nanotechnology*, 2013, **24**, 255305.

104. M. E. Kolewe, H. Park, C. Gray, X. Ye, R. Langer and L. E. Freed, *Adv. Mater.*, 2013, **25**, 4459-4465.

105. A. F. Christ, K. Franze, H. Gautier, P. Moshayedi, J. Fawcett, R. J. M. Franklin, R. T. Karadottir and J. Guck, *J. Biomech.*, 2010, **43**, 2986-2992.

106. P. Milovanovic, M. Djuric, O. Neskovic, D. Djonic, J. Potocnik, S. Nikolic, M. Stoiljkovic, V. Zivkovic and Z. Rakocevic, *Microsc. Microanal.*, 2013, **19**, 1341-1349.

107. C. Sato, F. A. Rodrigues, D. M. Garcia, C. M. P. Vidal, D. H. Pashley, L. Tjaederhane, M. R. Carrilho, F. D. Nascimento and I. L. S. Tersariol, *J. Dent. Res.*, 2013, **92**, 187-192.

108. Hadi T. Nia, Iman S. Bozchalooi, Y. Li, L. Han, H.-H. Hung, E. Frank, K. Youcef-Toumi, C. Ortiz and A. Grodzinsky, *Biophys. J.*, 2013, **104**, 1529-1537.

109. R. Hemmer, A. Hall, R. Spaulding, B. Rossow, M. Hester, M. Caroway, A. Haskamp, S. Wall, H. Bullen, C. Morris and K. Haik, *Molecules*, 2013, **18**, 11537-11552.

110. G. Balooch, G. W. Marshall, S. J. Marshall, O. L. Warren, S. A. S. Asif and M. Balooch, *J. Biomech.*, 2004, **37**, 1223-1232.

111. M. Stolz, R. Gottardi, R. Raiteri, S. Miot, I. Martin, R. Imer, U. Staufer, A. Raducanu, M. Düggelin, W. Baschong, A. U. Daniels, N. F. Friederich, A. Aszodi and U. Aebi, *Nat. Nanotechnol.*, 2009, **4**, 186-192.

112. D. J. Müller, A. Engel, U. Matthey, T. Meier, P. Dimroth and K. Suda, *J. Mol. Biol.*, 2003, **327**, 925-930.

113. S. F. M. van Dongen, J. Clerx, K. Norgaard, T. G. Bloemberg, J. Cornelissen, M. A. Trakselis, S. W. Nelson, S. J. Benkovic, A. E. Rowan and R. J. M. Nolte, *Nat. Chem.*, 2013, **5**, 945-951.

114. T. Ando, *Nanotechnology*, 2012, **23**, 062001.

115. M.-C. Giocondi, D. Yamamoto, E. Lesniewska, P.-E. Milhiet, T. Ando and C. Le Grimellec, *Biochim. Biophys. Acta, Biomembranes*, 2010, **1798**, 703-718.

116. A. San Paulo and R. Garcia, *Biophys. J.*, 2000, **78**, 1599-1605.

117. I. Liashkovich, W. Hafezi, J. E. Kuehn, H. Oberleithner, A. Kramer and V. Shahin, *J. Cell Sci.*, 2008, **121**, 2287-2292.

118. A. J. Malkin, A. McPherson and P. D. Gershon, *J. Virol.*, 2003, **77**, 6332-6340.

119. E. Soylemez, M. P. de Boer, U. Sae-Ueng, A. Evilevitch, T. A. Stewart and M. Nyman, *PLoS One*, 2013, **8**, e53601.

120. S. M. Lin, C. K. Lee, S. Y. Lee, C. L. Kao, C. W. Lin, A. B. Wang, S. M. Hsu and L. S. Huang, *Cell. Microbiol.*, 2005, **7**, 1763-1770.

121. J. Snijder, C. Uetrecht, R. J. Rose, R. Sanchez-Eugenia, G. A. Marti, J. Agirre, D. M. A. Guérin, G. J. L. Wuite, A. J. R. Heck and W. H. Roos, *Nat. Chem.*, 2013, **5**, 502-509.

122. Y. G. Kuznetsov, J. G. Victoria, W. E. Robinson and A. McPherson, *J. Virol.*, 2003, **77**, 11896-11909.

123. I. A. T. Schaap, F. Eghiaian, A. des Georges and C. Veigel, *J. Biol. Chem.*, 2012, **287**, 41078-41088.

124. G. A. Marti, M. G. Echeverria, M. L. Susevich, J. J. Becnel, S. A. Pelizza and J. J. Garcia, *J. Invertebr. Pathol.*, 2009, **102**, 233-237.

125. A. Rassi, Jr., A. Rassi and J. A. Marin-Neto, *Lancet*, 2010, **375**, 1388-1402.

126. J. Adamcik, J.-M. Jung, J. Flakowski, P. De Los Rios, G. Dietler and R. Mezzenga, *Nat. Nanotechnol.*, 2010, **5**, 423-428.

127. J. Legleiter, E. Mitchell, G. P. Lotz, E. Sapp, C. Ng, M. DiFiglia, L. M. Thompson and P. J. Muchowski, *J. Biol. Chem.*, 2010, **285**, 14777-14790.

128. Y. J. Zhu, H. Lin and R. Lal, *FASEB J.*, 2000, **14**, 1244-1254.

129. M. Arimon, I. Díez-Pérez, M. J. Kogan, N. Durany, E. Giralt, F. Sanz and X. Fernàndez-Busquets, *FASEB J.*, 2005, **19**, 1344-1346.

130. B. D. Trapp, J. Peterson, R. M. Ransohoff, R. Rudick, S. Mork and L. Bo, *New Eng. J. Med.*, 1998, **338**, 278-285.

131. J. H. Rand, X. X. Wu, A. S. Quinn, P. J. P. Chen, K. R. McCrae, E. G. Bovill and D. J. Taatjes, *Am. J. Pathol.*, 2003, **163**, 1193-1200.

132. I. Reviakine, W. Bergsma-Schutter and A. Brisson, *J. Struct. Biol.*, 1998, **121**, 356-362.

133. K.-H. Jeong, T.-W. Lee, C.-G. Ihm, J.-Y. Moon, G.-J. Lee, H.-K. Park and S.-H. Lee, *Kidney Blood Press. Res.*, 2012, **35**, 573-582.

134. A. Brodehl, P. N. Hedde, M. Dieding, A. Fatima, V. Walhorn, S. Gayda, T. Saric, B. Klauke, J. Gummert, D. Anselmetti, M. Heilemann, G. U. Nienhaus and H. Milting, *J. Biol. Chem.*, 2012, **287**, 16047-16057.

135. V. Karagkiozaki, P. G. Karagiannidis, N. Kalfagiannis, P. Kavatzikidou, P. Patsalas, D. Georgiou and S. Logothetidis, *Int. J. Nanomedicine*, 2012, **7**, 6063-6076.

136. G.-J. Lee, J. H. Jeong, S. Lee, S. Choi, Y. K. Pak, W. Kim and H.-K. Park, *Micron*, 2013, **44**, 167-173.

137. E. Pretorius, M.-J. Engelbrecht and W. Duim, *Ultrastruct. Pathol.*, 2012, **36**, 19-22.

138. P. Padmavathi, V. D. Reddy, P. Maturu and N. Varadacharyulu, *J. Atheroscler. Thromb.*, 2010, **17**, 619-627.

139. H. Oberleithner, *Pflugers. Arch.*, 2013, **465**, 1451-1458.

140. S. E. Cross, Y.-S. Jin, J. Rao and J. K. Gimzewski, *Nat. Nanotechnol.*, 2007, **2**, 780-783.

141. S. Kumar and V. M. Weaver, *Cancer Metastasis Rev.*, 2009, **28**, 113-127.

142. F. Braet, C. Seynaeve, R. De Zanger and E. Wisse, *J. Microsc.*, 1998, **190**, 328-338.

143. C. C. DuFort, M. J. Paszek and V. M. Weaver, *Nature Rev. Mol. Cell Biol.*, 2011, **12**, 308-319.

144. J. Friedrichs, A. Taubenberger and D. J. Müller, *J. Mol. Biol.*, 2007, **372**, 594-607.

145. K. Poole and D. Müller, *Br. J. Cancer*, 2005, **92**, 1499-1505.

146. N. P. Barrera, P. Herbert, R. M. Henderson, I. L. Martin and J. M. Edwardson, *Proc. Natl. Acad. Sci. U.S.A.*, 2005, **102**, 12595-12600.

147. C. Heu, A. Berquand, C. Elie-Caille and L. Nicod, *J. Struct. Biol.*, 2012, **178**, 1-7.

148. F. J. Giessibl, *Rev. Mod. Phys.*, 2003, **75**, 949-983.

149. Z. Reich, R. Kapon, R. Nevo, Y. Pilpel, S. Zmora and Y. Scolnik, *Biotechnol. Adv.*, 2001, **19**, 451-485.

150. B. Cappella and G. Dietler, *Surf. Sci. Rep.*, 1999, **34**, 1-104.

151. H.-J. Butt and M. Jaschke, *Nanotechnology*, 1995, **6**, 1.

152. H. Oberleithner, C. Riethmüller, T. Ludwig, V. Shahin, C. Stock, A. Schwab, M. Hausberg, K. Kusche and H. Schillers, *J. Cell Sci.*, 2006, **119**, 1926-1932.

153. H. Hertz, *J. Reine Angew. Math.*, 1881, **92**, 156-171.

154. A. M. Morris, M. A. Watzky and R. G. Finke, *Biochim. Biophys. Acta, Proteins Proteomics*, 2009, **1794**, 375-397.

155. R. E. Mahaffy, C. K. Shih, F. C. MacKintosh and J. Kas, *Phys. Rev. Lett.*, 2000, **85**, 880-883.

156. E. K. Dimitriadis, F. Horkay, J. Maresca, B. Kachar and R. S. Chadwick, *Biophys. J.*, 2002, **82**, 2798-2810.

157. M. McElfresh, E. Baesu, R. Balhorn, J. Belak, M. J. Allen and R. E. Rudd, *Proc. Natl. Acad. Sci. U.S.A.*, 2002, **99**, 6493-6497.

158. C. Rotsch, K. Jacobson and M. Radmacher, *Proc. Natl. Acad. Sci. U.S.A.*, 1999, **96**, 921-926.

159. C. M. Franz and P. H. Puech, *Cellular and Molecular Bioengineering*, 2008, **1**, 289-300.

160. J. Alcaraz, L. Buscemi, M. Grabulosa, X. Trepat, B. Fabry, R. Farre and D. Navajas, *Biophys. J.*, 2003, **84**, 2071-2079.

161. I. D. Medalsy and D. J. Müller, *ACS Nano*, 2013, **7**, 2642-2650.

162. C. Schäefer, Y. Ludwig, V. Shahin, A. Kramer, P. Carl, H. Schillers and H. Oberleithner, *Pflugers. Arch.*, 2007, **453**, 809-818.

163. W. A. Lam, M. J. Rosenbluth and D. A. Fletcher, *Blood*, 2007, **109**, 3505-3508.

164. C. K. M. Fung, K. Seiffert-Sinha, K. W. C. Lai, R. Yang, D. Panyard, J. Zhang, N. Xi and A. A. Sinha, *Nanomed. Nanotechnol. Biol. Med.*, 2010, **6**, 191-200.

165. P. Klingbeil, R. Marhaba, T. Jung, R. Kirmse, T. Ludwig and M. Zoeller, *Mol. Cancer Res.*, 2009, **7**, 168-179.

166. Y. Liu, M. A. Black, L. Caron and T. A. Camesano, *Biotechnol. Bioeng.*, 2006, **93**, 297-305.

167. P. Loskill, C. Zeitz, S. Grandthyll, N. Thewes, F. Mueller, M. Bischoff, M. Herrmann and K. Jacobs, *Langmuir*, 2013, **29**, 5528-5533.

168. C. E. Hills, T. Jin, E. Siamantouras, I. K. K. Liu, K. P. Jefferson and P. E. Squires, *PLoS One*, 2013, **8**, e71819.

169. C. D. Frisbie, L. F. Rozsnyai, A. Noy, M. S. Wrighton and C. M. Lieber, *Science*, 1994, **265**, 2071-2074.

170. G. U. Lee, D. A. Kidwell and R. J. Colton, *Langmuir*, 1994, **10**, 354-357.

171. G. U. Lee, L. A. Chrisey and R. J. Colton, *Science*, 1994, **266**, 771-773.

172. A. Noy, D. V. Vezenov and C. M. Lieber, *Annu. Rev. Mater. Sci.*, 1997, **27**, 381-421.

173. F. A. Carvalho, S. de Oliveira, T. Freitas, S. Goncalves and N. C. Santos, *PLoS One*, 2011, **6**, e18167.

174. P. Tripathi, A. Beaussart, D. Alsteens, V. Dupres, I. Claes, I. von Ossowski, W. M. de Vos, A. Palva, S. Lebeer, J. Vanderleyden and Y. F. Dufrene, *ACS Nano*, 2013, **7**, 3685-3697.

175. Q. Guo, Y. Xia, M. Sandig and J. Yang, *J. Biomech.*, 2012, **45**, 304-309.

176. W. F. Heinz and J. H. Hoh, *Trends Biotechnol.*, 1999, **17**, 143-150.

177. Y. F. Dufrêne, D. Martinez-Martin, I. Medalsy, D. Alsteens and D. J. Müller, *Nat. Methods*, 2013, **10**, 847-854.

178. I. Medalsy, U. Hensen and D. J. Müller, *Angew. Chem. Int. Ed.*, 2011, **50**, 12103-12108.

179. B. J. Albers, T. C. Schwendemann, M. Z. Baykara, N. Pilet, M. Liebmann, E. I. Altman and U. D. Schwarz, *Nanotechnology*, 2009, **20**, 264002.

180. M. Z. Baykara, T. C. Schwendemann, E. I. Altman and U. D. Schwarz, *Adv. Mater.*, 2010, **22**, 2838-2853.

181. L. Arnal, D. O. Serra, N. Cattelan, M. F. Castez, L. Vázquez, R. C. Salvarezza, O. M. Yantorno and M. E. Vela, *Langmuir*, 2012, **28**, 7461-7469.

182. K. Sweers, K. van der Werf, M. Bennink and V. Subramaniam, *Nanoscale Res. Lett.*, 2011, **6**, 270.

183. S. Wegmann, I. D. Medalsy, E. Mandelkow and D. J. Müller, *Proc. Natl. Acad. Sci. U.S.A.*, 2013, **110**, E313-E321.

184. J. Liu, N. Sun, M. A. Bruce, J. C. Wu and M. J. Butte, *PLoS One*, 2012, **7**, e37559.

185. E. Dague, D. Alsteens, J. P. Latgé, C. Verbelen, D. Raze, A. R. Baulard and Y. F. Dufrêne, *Nano Lett.*, 2007, **7**, 3026-3030.

186. G. Lama, M. Papi, C. Angelucci, G. Maulucci, G. Sica and M. De Spirito, *PLoS One*, 2013, **8**.

187. D. Alsteens, M. C. Garcia, P. N. Lipke and Y. F. Dufrene, *Proc. Natl. Acad. Sci. U.S.A.*, 2010, **107**, 20744-20749.

188. S. Moreno-Flores and J. L. Toca-Herrera, *Hybridizing Surface Probe Microscopies: Toward a Full Description of the Meso- and Nanoworlds*, CRC Press Taylor & Francis Group, Boca Raton, 2013.

189. S. M. Flores and J. L. Toca-Herrera, *Nanoscale*, 2009, **1**, 40-49.

190. C. Kranz, *Analyst*, 2014, **139**, 336-352.

191. E. Casero, L. Vázquez, A. M. Parra-Alfambra and E. Lorenzo, *Analyst*, 2010, **135**, 1878-1903.

192. S. Kalinin and A. Gruverman, eds., *Scanning Probe Microscopy: Electrical and Electromechanical Phenomena at the Nanoscale*, Springer, New York, 2007.

193. C. Callies, P. Schön, I. Liashkovich, C. Stock, K. Kusche-Vihrog, J. Fels, A. S. Straeter and H. Oberleithner, *Nanotechnology*, 2009, **20**, 175104.

194. E. Hecht, K. Thompson, M. Frick, O. H. Wittekindt, P. Dietl, B. Mizaikoff and C. Kranz, *Anal. Chem.*, 2012, **84**, 5716-5722.

195. L. Bastatas, D. Martinez-Marin, J. Matthews, J. Hashem, Y. J. Lee, S. Sennoune, S. Filleur, R. Martinez-Zaguilan and S. Park, *Biochim. Biophys. Acta, General Subjects*, 2012, **1820**, 1111-1120.

196. K. B. Szarama, N. Gavara, R. S. Petralia, M. W. Kelley and R. S. Chadwick, *Development*, 2012, **139**, 2187-2197.

197. W. C. Lin, C. D. Blanchette, T. V. Ratto and M. L. Longo, *Biophys. J.*, 2006, **90**, 228-237.

198. A. B. Mathur, G. A. Truskey and W. M. Reichert, *Biophys. J.*, 2000, **78**, 1725-1735.

199. H. G. Franquelim, D. Gaspar, A. S. Veiga, N. C. Santos and M. Castanho, *Biochim. Biophys. Acta, Biomembranes*, 2013, **1828**, 1777-1785.

200. G. M. Lopez-Ayon, D. J. Oliver, P. H. Grutter and S. V. Komarova, *Microsc. Microanal.*, 2012, **18**, 808-815.

201. E. Hecht, P. Knittel, E. Felder, P. Dietl, B. Mizaikoff and C. Kranz, *Analyst*, 2012, **137**, 5208-5214.

202. Y. Suzuki, N. Sakai, A. Yoshida, Y. Uekusa, A. Yagi, Y. Imaoka, S. Ito, K. Karaki and K. Takeyasu, *Sci. Rep.*, 2013, **3**, 2131.

203. S. Fukuda, T. Uchihashi, R. Iino, Y. Okazaki, M. Yoshida, K. Igarashi and T. Ando, *Rev. Sci. Instrum.*, 2013, **84**, 073706.

204. E. H. Synge, in *Philosophical Magazine*, 1928, vol. 6, pp. 356-362.

205. D. W. Pohl, W. Denk and M. Lanz, *Appl. Phys. Lett.*, 1984, **44**, 651-653.

206. A. Lewis, M. Isaacson, A. Harootunian and A. Muray, *Ultramicroscopy*, 1984, **13**, 227-231.

207. N. Courjon, *Near-Field Micrscopy and Near-Field Optics*, Imperial College Press, London, 2003.

208. H. Muramatsu, N. Chiba, T. Ataka, S. Iwabuchi, N. Nagatani, E. Tamiya and M. Fujihira, *Opt. Rev.*, 1996, **3**, 470-474.

209. A. Harder, M. Dieding, V. Walhorn, S. Degenhard, A. Brodehl, C. Wege, H. Milting and D. Anselmetti, *Beilstein J. Nanotechnol.*, 2013, **4**, 510-516.

210. J. M. Kim, T. Ohtani and H. Muramatsu, *Surf. Sci.*, 2004, **549**, 273-280.

211. R. C. Dunn, *Chem. Rev.*, 1999, **99**, 2891-2928.

212. A. Hartschuh, *Angew. Chem. Int. Ed.*, 2008, **47**, 8178-8191.

213. S. Kirstein, *Curr. Opin. Colloid Interface Sci.*, 1999, **4**, 256-264.

214. J. M. Kim, T. Ohtani, S. Sugiyama, T. Hirose and H. Muramatsu, *Anal. Chem.*, 2001, **73**, 5984-5991.

215. P. N. Minh, T. Ono and M. Esashi, *Rev. Sci. Instrum.*, 2000, **71**, 3111-3117.

216. H. Zhou, A. Midha, G. Mills, L. Donaldson and J. M. R. Weaver, *Appl. Phys. Lett.*, 1999, **75**, 1824-1826.

217. N. F. Vanhulst, M. H. P. Moers, O. F. J. Noordman, R. G. Tack, F. B. Segerink and B. Bolger, *Appl. Phys. Lett.*, 1993, **62**, 461-463.

218. G. Carbone, B. Zappone, R. Barberi and R. Bartolino, *Mol. Cryst. Liquid Cryst.*, 2002, **372**, 373-382.

219. M. Sackrow, C. Stanciu, M. A. Lieb and A. J. Meixner, *Chemphyschem*, 2008, **9**, 316-320.

220. W.-S. Chang, S. Bauerdick and M. S. Jeong, *Ultramicroscopy*, 2008, **108**, 1070-1075.

221. J. Kim, T. Hirose, S. Sugiyama, T. Ohtani and H. Muramatsu, *Nano Lett.*, 2004, **4**, 2091-2097.

222. E. Kimura, J. Hitomi and T. Ushiki, *Arch. Histol. Cytol.*, 2002, **65**, 435-444.

223. C.-C. Chen, Y. Zhou and L. A. Baker, *Annu. Rev. Anal. Chem.*, 2012, **5**, 207-228.

224. P. K. Hansma, B. Drake, O. Marti, S. A. C. Gould and C. B. Prater, *Science*, 1989, **243**, 641-643.

225. C. A. Morris, A. K. Friedman and L. A. Baker, *Analyst*, 2010, **135**, 2190-2202.

226. Y. E. Korchev, C. L. Bashford, M. Milovanovic, I. Vodyanoy and M. J. Lab, *Biophys. J.*, 1997, **73**, 653-658.

227. J. K. H. Hörber, J. Mosbacher, W. Haberle, J. P. Ruppersberg and B. Sakmann, *Biophys. J.*, 1995, **68**, 1687-1693.

228. R. Proksch, R. Lal, P. K. Hansma, D. Morse and G. Stucky, *Biophys. J.*, 1996, **71**, 2155-2157.

229. R. Lal and H. Lin, *Microsc. Res. Tech.*, 2001, **52**, 273-288.

230. NanoFountainpens™ for Gas or Chemical Delivery. http://www.nanonics.co.il/products/spm-probes-and-nanotools/afm-probes/nanofountainpens-for-gas-or-chemical-delivery.html (accessed Nov 18, 2013).

231. A. Meister, M. Gabi, P. Behr, P. Studer, J. Vörös, P. Niedermann, J. Bitterli, J. Polesel-Maris, M. Liley, H. Heinzelmann and T. Zambelli, *Nano Lett.*, 2009, **9**, 2501-2507.

232. J. Rheinlaender and T. E. Schäeffer, *Soft Matter*, 2013, **9**, 3230-3236.

233. J. Heinze, *Angew. Chem. Int. Ed.*, 1993, **32**, 1268-1288.

234. A. J. Bard, F. R. F. Fan, J. Kwak and O. Lev, *Anal. Chem.*, 1989, **61**, 132-138.

235. A. J. Bard, F. R. F. Fan, D. T. Pierce, P. R. Unwin, D. O. Wipf and F. M. Zhou, *Science*, 1991, **254**, 68-74.

236. C. Lee, J. Y. Kwak and F. C. Anson, *Anal. Chem.*, 1991, **63**, 1501-1504.

237. S. Amemiya, A. J. Bard, F.-R. F. Fan, M. V. Mirkin and P. R. Unwin, *Annu. Rev. Anal. Chem.*, 2008, **1**, 95-131.

238. A. J. Bard, X. Li and W. Zhan, *Biosens. Bioelectron.*, 2006, **22**, 461-472.

239. I. Beaulieu, S. Kuss, J. Mauzeroll and M. Geissler, *Anal. Chem.*, 2011, **83**, 1485-1492.

240. S. Bergner, P. Vatsyayan and F.-M. Matysik, *Anal. Chim. Acta*, 2013, **775**, 1-13.

241. R. E. Gyurcsanyi, G. Jagerszki, G. Kiss and K. Toth, *Bioelectrochemistry*, 2004, **63**, 207-215.

242. T. Matsue, *Anal. Sci.*, 2013, **29**, 171-179.

243. W. S. Roberts, D. J. Lonsdale, J. Griffiths and S. P. J. Higson, *Biosens. Bioelectron.*, 2007, **23**, 301-318.

244. P. Sun, F. O. Laforge and M. V. Mirkin, *PCCP*, 2007, **9**, 802-823.

245. J. V. Macpherson and P. R. Unwin, *Anal. Chem.*, 2000, **72**, 276-285.

246. A. Kueng, C. Kranz, A. Lugstein, E. Bertagnolli and B. Mizaikoff, *Angew. Chem. Int. Ed.*, 2003, **42**, 3238-3240.

247. A. Kueng, C. Kranz, B. Mizaikoff, A. Lugstein and E. Bertagnolli, *Appl. Phys. Lett.*, 2003, **82**, 1592-1594.

248. J. V. Macpherson, P. R. Unwin, A. C. Hillier and A. J. Bard, *J. Am. Chem. Soc.*, 1996, **118**, 6445-6452.

249. M. A. Derylo, K. C. Morton and L. A. Baker, *Langmuir*, 2011, **27**, 13925-13930.

250. J. T. Cox and B. Zhang, *Annu. Rev. Anal. Chem.*, 2012, **5**, 253-272.

251. J. Abbou, C. Demaille, M. Druet and J. Moiroux, *Anal. Chem.*, 2002, **74**, 6355-6363.

252. C. Kranz, G. Friedbacher and B. Mizaikoff, *Anal. Chem.*, 2001, **73**, 2491-2500.

253. P. S. Dobson, J. M. R. Weaver, M. N. Holder, P. R. Unwin and J. V. Macpherson, *Anal. Chem.*, 2005, **77**, 424-434.

254. M. R. Gullo, P. L. T. M. Frederix, T. Akiyama, A. Engel, N. F. deRooij and U. Staufer, *Anal. Chem.*, 2006, **78**, 5436-5442.

255. A. Lugstein, E. Bertagnolli, C. Kranz and B. Mizaikoff, *Surf. Interface Anal.*, 2002, **33**, 146-150.

256. R. J. Fasching, Y. Tao and F. B. Prinz, *Sens. Actuators, B*, 2005, **108**, 964-972.

257. H. Shin, P. J. Hesketh, B. Mizaikoff and C. Kranz, *Anal. Chem.*, 2007, **79**, 4769-4777.

258. J. Wiedemair, B. Balu, J.-S. Moon, D. W. Hess, B. Mizaikoff and C. Kranz, *Anal. Chem.*, 2008, **80**, 5260-5265.

259. Y. Hirata, S. Yabuki and F. Mizutani, *Bioelectrochemistry*, 2004, **63**, 217-224.

260. C. Kranz, A. Kueng, A. Lugstein, E. Bertagnolli and B. Mizaikoff, *Ultramicroscopy*, 2004, **100**, 127-134.

261. S. Sekine, H. Kaji and M. Nishizawa, *Anal. Bioanal. Chem.*, 2008, **391**, 2711-2716.

262. A. J. Wain, D. Cox, S. Zhou and A. Turnbull, *Electrochem. Commun.*, 2011, **13**, 78-81.

263. M. Salomo, S. E. Pust, G. Wittstock and E. Oesterschulze, *Microelectron. Eng.*, 2010, **87**, 1537-1539.

264. J. V. Macpherson, C. E. Jones, A. L. Barker and P. R. Unwin, *Anal. Chem.*, 2002, **74**, 1841-1848.

265. D. P. Burt, N. R. Wilson, J. M. R. Weaver, P. S. Dobson and J. V. Macpherson, *Nano Lett.*, 2005, **5**, 639-643.

266. W. Smirnov, A. Kriele, R. Hoffmann, E. Sillero, J. Hees, O. A. Williams, N. Yang, C. Kranz and C. E. Nebel, *Anal. Chem.*, 2011, **83**, 4936-4941.

267. J. Wiedemair, J.-S. Moon, F. Reinauer, B. Mizaikoff and C. Kranz, *Electrochem. Commun.*, 2010, **12**, 989-991.

268. A. Davoodi, J. Pan, C. Leygraf and S. Norgren, *Electrochem. Solid-State Lett.*, 2005, **8**, B21-B24.

269. S. E. Pust, M. Salomo, E. Oesterschulze and G. Wittstock, *Nanotechnology*, 2010, **21**, 105709.

270. H. Shin, P. J. Hesketh, B. Mizaikofff and C. Kranz, *Sens. Actuators, B*, 2008, **134**, 488-495.

271. A. Anne, E. Cambril, A. Chovin, C. Demaille and C. Goyer, *ACS Nano*, 2009, **3**, 2927-2940.

272. A. Anne, A. Chovin, C. Demaille and M. Lafouresse, *Anal. Chem.*, 2011, **83**, 7924-7932.

273. K. Huang, A. Anne, M. A. Bahri and C. Demaille, *ACS Nano*, 2013, **7**, 4151-4163.

274. A. Anne, C. Demaille and C. Goyer, *ACS Nano*, 2009, **3**, 819-827.

275. K. Wang, C. Goyer, A. Anne and C. Demaille, *J. Phys. Chem. B*, 2007, **111**, 6051-6058.

276. Y. Takahashi, A. I. Shevchuk, P. Novak, B. Babakinejad, J. Macpherson, P. R. Unwin, H. Shiku, J. Gorelik, D. Klenerman, Y. E. Korchev and T. Matsue, *Proc. Natl. Acad. Sci. U.S.A.*, 2012, **109**, 11540-11545.

277. A. Ueda, O. Niwa, K. Maruyama, Y. Shindo, K. Oka and K. Suzuki, *Angew. Chem. Int. Ed.*, 2007, **46**, 8238-8241.

278. J. Rheinlaender, N. A. Geisse, R. Proksch and T. E. Schäeffer, *Langmuir*, 2011, **27**, 697-704.

279. F. Ghorbani-Bidkorbeh, S. Shahrokhian, A. Mohammadi and R. Dinarvand, *J. Electroanal. Chem.*, 2010, **638**, 212-217.

280. L. Wildling, C. Rankl, T. Haselgrübler, H. J. Gruber, M. Holy, A. H. Newman, M.-F. Zou, R. Zhu, M. Freissmuth, H. H. Sitte and P. Hinterdorfer, *J. Biol. Chem.*, 2012, **287**, 105-113.

281. J. D. Beard, R. H. Guy and S. N. Gordeev, *J. Invest. Dermatol.*, 2013, **133**, 1565-1571.

282. R. R. Damerla, K. E. Knickelbein, S. Strutt, F.-J. Liu, H. Wang and P. L. Opresko, *Cell Cycle*, 2012, **11**, 3036-3044.

283. H.-Y. Lee, L. Han, P. J. Roughley, A. J. Grodzinsky and C. Ortiz, *J. Struct. Biol.*, 2013, **181**, 264-273.

284. C. Y. Wen, C. B. Wu, B. Tang, T. Wang, C. H. Yan, W. W. Lu, H. Pan, Y. Hu and K. Y. Chiu, *Osteoarthr. Cartil.*, 2012, **20**, 916-922.

285. M. Hayley, S. Bourbigot and V. Booth, *PLoS One*, 2011, **6**, 1-6.

286. S. Irman, S. Miha, M. Igor, B. Rozman and B. Bozic, *Autoimmunity*, 2009, **42**, 414-423.

287. S. Irman, M. Skarabot, I. Musevic, B. Rozman and B. Bozic, *J. Autoimmun.*, 2011, **36**, 98-105.

288. M. S. Kim, J. Kim, W. Lee, S.-J. Cho, J.-M. Oh, J.-Y. Lee, S. Baek, Y. J. Kim, T. S. Sim, H. J. Lee, G.-E. Jung, S.-I. Kim, J.-M. Park, J. H. Oh, O. Gurel, S. S. Lee and J.-G. Lee, *Small*, 2013, **9**, 3103-3110.

289. M. Li, L. Liu, N. Xi, Y. Wang, X. Xiao and W. Zhang, *Biochem. Biophys. Res. Commun.*, 2013, **438**, 709-714.

290. M. Li, X. Xiao, L. Liu, N. Xi, Y. Wang, Z. Dong and W. Zhang, *J. Mol. Recognit.*, 2013, **26**, 432-438.

291. M. Li, X. Xiao, L. Liu, N. Xi, Y. Wang, Z. Dong and W. Zhang, *Scanning*, 2013, **35**, 40-46.

292. K. J. Reeves, J. Hou, S. E. Higham, Z. Sun, J. P. Trzeciakowski, G. A. Meininger and N. J. Brown, *Nanomedicine*, 2013, **8**, 921-934.

293. M. K. Sewell-Loftin, C. B. Brown, H. S. Baldwin and W. D. Merryman, *J. Heart Valve Dis.*, 2012, **21**, 513-520.

294. K. He, X. Shi, X. Zhang, S. Dang, X. Ma, F. Liu, M. Xu, Z. Lv, D. Han, X. Fang and Y. Zhang, *Cardiovasc. Res.*, 2011, **92**, 39-47.

295. B. Stäedler, T. M. Bläettler and A. Franco-Obregon, *J. Microsc.*, 2010, **237**, 63-69.

296. J.-S. Lee, W. J. Cho, K. Jeftinija, S. Jeftinija and B. P. Jena, *J. Cell Mol. Med.*, 2009, **13**, 365-372.

297. R. Mezencev, L. Wang, W. Xu, B. Kim, T. A. Sulchek, G. W. Daneker and J. F. McDonald, *Anticancer Drugs*, 2013, **24**, 504-518.

298. K. Yanamandra, O. Alexeyev, V. Zamotin, V. Srivastava, A. Shchukarev, A.-C. Brorsson, G. G. Tartaglia, T. Vogl, R. Kayed, G. Wingsle, J. Olsson, C. M. Dobson, A. Bergh, F. Elgh and L. A. Morozova-Roche, *PLoS One*, 2009, **4**, e5562.

299. S. Zhang, M. Andreasen, J. T. Nielsen, L. Liu, E. H. Nielsen, J. Song, G. Ji, F. Sun, T. Skrydstrup, F. Besenbacher, N. C. Nielsen, D. E. Otzen and M. Dong, *Proc. Natl. Acad. Sci. U.S.A.*, 2013, **110**, 2798-2803.

300. N. Buzhynskyy, J.-F. Girmens, W. Faigle and S. Scheuring, *J. Mol. Biol.*, 2007, **374**, 162-169.

301. R. Creasey, S. Sharma, C. T. Gibson, J. E. Craig, A. Ebner, T. Becker, P. Hinterdorfer and N. H. Voelcker, *Ultramicroscopy*, 2011, **111**, 1055-1061.

302. N. M. Haralampus-Grynaviski, L. E. Lamb, C. M. R. Clancy, C. Skumatz, J. M. Burke, T. Sarna and J. D. Simon, *Proc. Natl. Acad. Sci. U.S.A.*, 2003, **100**, 3179-3184.

303. S. Kawamura, A. T. Colozo, L. Ge, D. J. Mueller and P. S. H. Park, *J. Biol. Chem.*, 2012, **287**, 21826-21835.

304. S. Kotova, C. Vijayasarathy, E. K. Dimitriadis, L. Ikonomou, H. Jaffe and P. A. Sieving, *Biochemistry*, 2010, **49**, 7023-7032.

305. J. A. Last, T. Pan, Y. Ding, C. M. Reilly, K. Keller, T. S. Acott, M. P. Fautsch, C. J. Murphy and P. Russell, *Invest. Ophthalmol. Vis. Sci.*, 2011, **52**, 2147-2152.

306. K. R. Cho, Y. Huang, S. Yu, S. Yin, M. Plomp, S. R. Qiu, R. Lakshminarayanan, J. Moradian-Oldak, M.-S. Sy and J. J. De Yoreo, *J. Am. Chem. Soc.*, 2011, **133**, 8586-8593.

307. T. Yoshino, S. Sugiyama, S. Hagiwara, D. Fukushi, M. Shichiri, H. Nakao, J. M. Kim, T. Hirose, H. Muramatsu and T. Ohtani, *Ultramicroscopy*, 2003, **97**, 81-87.

308. M. de Jager, J. van Noort, D. C. van Gent, C. Dekker, R. Kanaar and C. Wyman, *Mol. Cell*, 2001, **8**, 1129-1135.

309. D. Alsteens, H. Trabelsi, P. Soumillion and Y. F. Dufrene, *Nature Communications*, 2013, **4**.

310. V. Dupres, F. D. Menozzi, C. Locht, B. H. Clare, N. L. Abbott, S. Cuenot, C. Bompard, D. Raze and Y. F. Dufrene, *Nat. Methods*, 2005, **2**, 515-520.

311. I. E. Ivanov, E. N. Kintz, L. A. Porter, J. B. Goldberg, N. A. Burnham and T. A. Camesano, *J. Bacteriol.*, 2011, **193**, 1259-1266.

312. A. Aloisi, A. Barca, A. Romano, S. Guerrieri, C. Storelli, R. Rinaldi and T. Verri, *PLoS One*, 2013, **8**, e68159.

313. K. A. Conway, S. J. Lee, J. C. Rochet, T. T. Ding, R. E. Williamson and P. T. Lansbury, *Proc. Natl. Acad. Sci. U.S.A.*, 2000, **97**, 571-576.

314. T. Kowalewski and D. M. Holtzman, *Proc. Natl. Acad. Sci. U.S.A.*, 1999, **96**, 3688-3693.

315. M. Cárdenas, U. Elofsson and L. Lindh, *Biomacromolecules*, 2007, **8**, 1149-1156.

316. C. Hegedus, T. Bistey, E. Flora-Nagy, G. Keszthelyi and A. Jenei, *J. Dent.*, 1999, **27**, 509-515.

317. G. W. Marshall, M. Balooch, R. R. Gallagher, S. A. Gansky and S. J. Marshall, *J. Biomed. Mater. Res*, 2001, **54**, 87-95.

318. R. Mohan, S. Agrawal and M. Gundappa, *Cont. Clin. Den.*, 2013, **4**, 286-294.

319. B. Chasan, N. A. Geisse, K. Pedatella, D. G. Wooster, M. Teintze, M. D. Carattino, W. H. Goldmann and H. F. Cantiello, *Eur. Biophys. J.*, 2002, **30**, 617-624.

320. F. Liu and D. J. Tschumperlin, *J. Vis. Exp.*, 2011, e2911.

321. R. Manzenreiter, F. Kienberger, V. Marcos, K. Schilcher, W. D. Krautgartner, A. Obermayer, M. Huml, W. Stoiber, A. Hector, M. Griese, M. Hannig, M. Studnicka, L. Vitkov and D. Hart, *J. Cyst. Fibros.*, 2012, **11**, 84-92.

322. X. Trepat, M. Grabulosa, F. Puig, G. N. Maksym, D. Navajas and R. Farre, *Am. J. Physiol. Lung Cell Mol. Physiol.*, 2004, **287**, L1025-L1034.

323. I. A. Alvi, J. Madan, D. Kaushik, S. Sardana, R. S. Pandey and A. Ali, *Anticancer Drugs*, 2011, **22**, 774-782.

324. Y. Fu, Y. Zu, L. Chen, T. Efferth, H. Liang, Z. Liu and W. Liu, *Planta Med.*, 2007, **73**, 1275-1280.

325. K. S. Kim, M. K. Shin, J. H. Kim, M. H. Kim, C.-R. Haw and H.-K. Park, *Microsc. Res. Tech.*, 2012, **75**, 620-625.

326. M. K. Shin, K. S. Kim, J. J. Ahn, N. I. Kim, H. K. Park and C. R. Haw, *Clin. Exp. Dermatol.*, 2012, **37**, 156-163.

327. H. G. Franquelim, D. Gaspar, A. Salome Veiga, N. C. Santos and M. A. R. B. Castanho, *Biochim. Biophys. Acta, Biomembranes*, 2013, **1828**, 1777-1785.

328. S. Guy, D. Rotem, Z. Hayouka, R. Gabizon, A. Levin, L. Zemel, A. Loyter, D. Porath and A. Friedler, *Chem. Commun.*, 2013, **49**, 3113-3115.

329. Y. J. Jung, J. A. Albrecht, J.-W. Kwak and J. W. Park, *Nucleic Acids Res.*, 2012, **40**, 11728-11736.

FIGURES

Disease/Disorder Category	Selected References
Addiction	162, 168, 279, 280

Aging	63, 106, 111, 281-284
Autoimmune diseases	78, 131, 285-287
Cancer	8, 140, 146, 186, 195, 201, 288-292
Cardiovascular diseases	18, 80, 131-136, 139, 173, 184, 193, 293-295
Endocrine and exocrine system diseases	10, 152, 296-299
Eye diseases	12, 300-305
Genetic disorders	127, 210, 214, 221, 222, 306-308
Microbial infections	9, 174, 187, 309-311
Neurological disorders	17, 105, 125, 126, 128, 129, 182, 183, 312-314
Oral health	9, 107, 167, 315-318
Respiratory system diseases	13, 160, 165, 181, 194, 319-322
Skin diseases	1, 2, 147, 164, 323-326
Viral infections	3, 11, 117-123, 327-329

Table 1. Selected atomic force microscopy studies which pertain to the listed disease/disorder categories

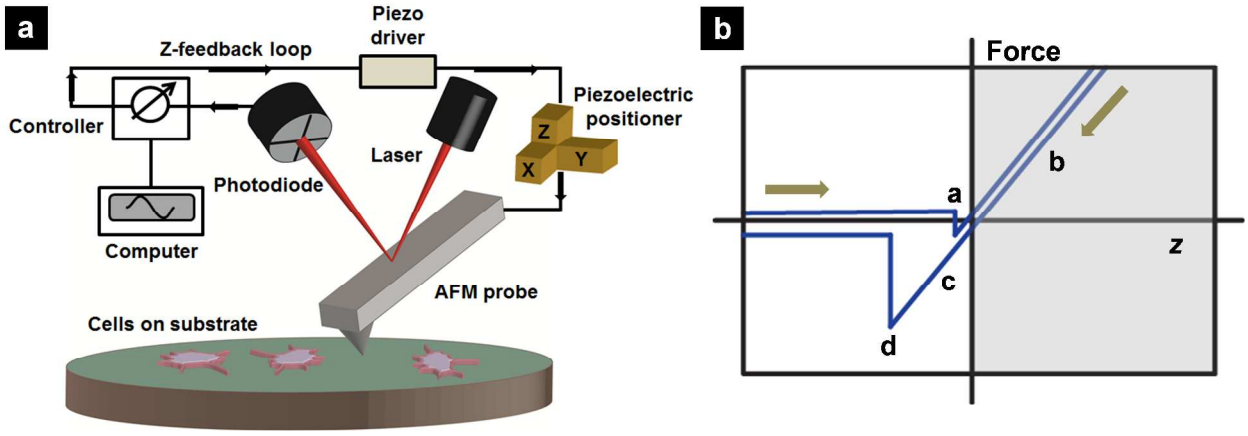

Figure 1. a Schematic of an atomic force microscope instrumental set-up. **b** A schematic of an example force-distance curve where force, calculated from cantilever deflection, is plotted vs. tip-surface distance (*z*). At long tip–substrate distances, the overall force felt by the tip is almost zero (left-side of the plot). As the tip approaches the surface, atoms between the probe and the substrate begin to experience attractive van der Waals forces and the tip will abruptly snap into contact with the surface (noted as 'a'). The tip experiences a repulsive force regime once in contact with the surface (noted as 'b'). In ambient conditions, when the tip is retracted (noted as 'c'), water or solvent that is inevitably present on both the surface and the tip experiences an attractive, capillary force. Once the tip snaps off the surface (noted as 'd'), forces which act on the tip are zero again.

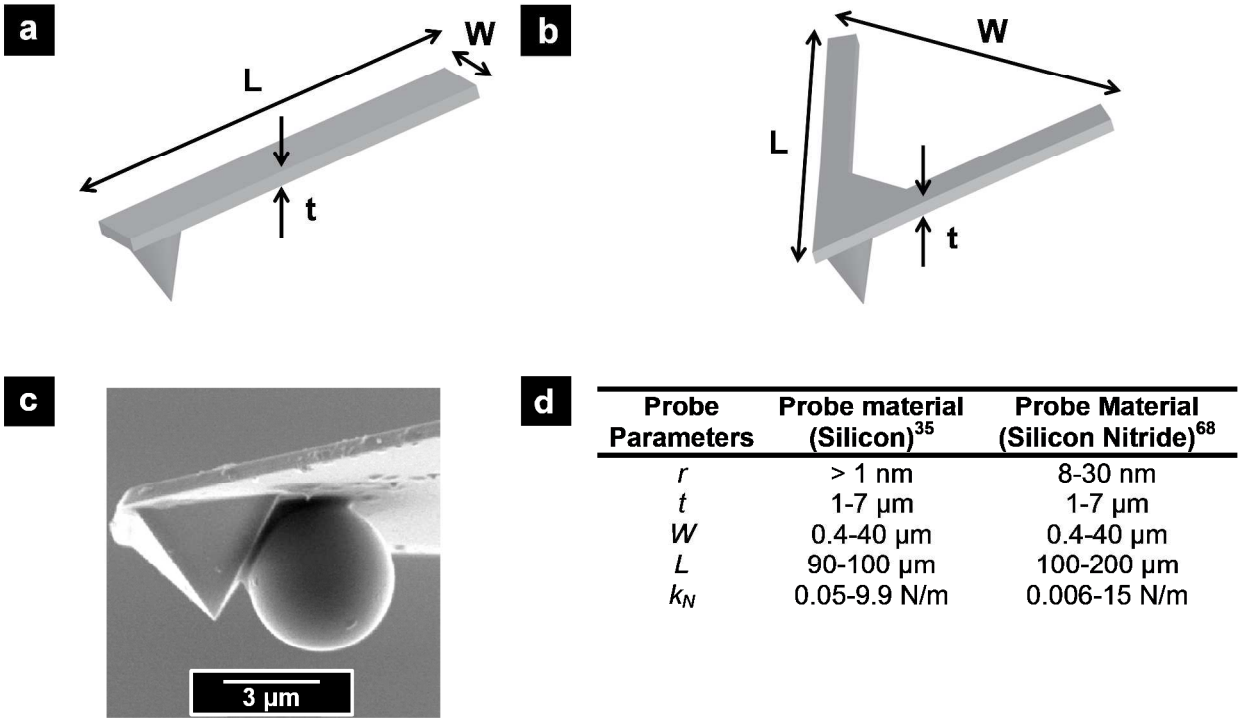

d

Probe Parameters	Probe material (Silicon)[35]	Probe Material (Silicon Nitride)[68]
r	> 1 nm	8-30 nm
t	1-7 µm	1-7 µm
W	0.4-40 µm	0.4-40 µm
L	90-100 µm	100-200 µm
k_N	0.05-9.9 N/m	0.006-15 N/m

Figure 2 Typical geometries of commercially available silicon (**a**) and silicon nitride (**b**) atomic force microscopy (AFM) probes used in contact and intermittent contact modes, respectively, where *L* is the length of the cantilever, *W* is the width of the AFM probe chip and *t* is the thickness of the cantilever. **c** A scanning electron microscopy image of a 5 µm diameter silica particle glued to an AFM probe cantilever, behind the silicon tip. These types of probes can be advantageous when making point-force measurements on cellular samples in many instances due to the large surface area of the probe. (Reprinted with permission from ref. 63 with permission from Institute of Physics. doi: 10.1088/0031-9155/50/1/007). **d** A table of selected AFM probe parameters for commercially-available silicon and silicon nitride probes, where *r*, *t*, *W*, *L* and k_N are the tip radius, cantilever thickness, cantilever width, cantilever length and probe spring constant, respectively.

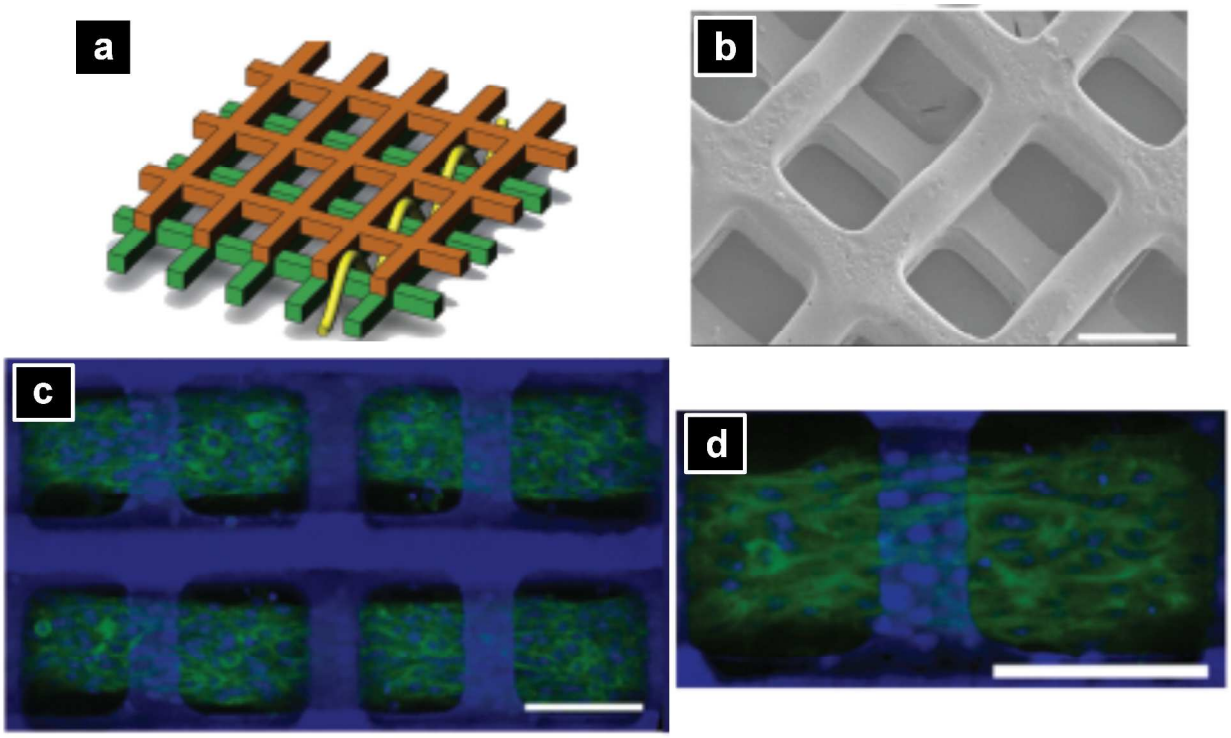

Figure 3a A schematic of an overlapping planar, poly-(glycerol sebacate) elastomeric scaffold fabricated to mimic native tissue. The yellow line represents the pore connectivity pattern. **b** A scanning electron microscopy image of the internal pore structure within the elastomeric scaffold shown schematically in **a**. Each sheet is approximately 70 μm thick and contains rectangular pores that are 250 x 70 μm^2. **c** A confocal microscopy image of murine skeletal myoblast cells cultured on the scaffold. F-actin was stained (green) and cell nuclei are counterstained (blue). **d** A zoom-in view of a multi-cellular bundle, shown in **c**, which is aligned with the scaffold. White scale bar in all images represent 100 μm. (Reprinted with permission from ref. 104 with permission from Wiley-VCH. doi: 10.1002/adma.201301016).

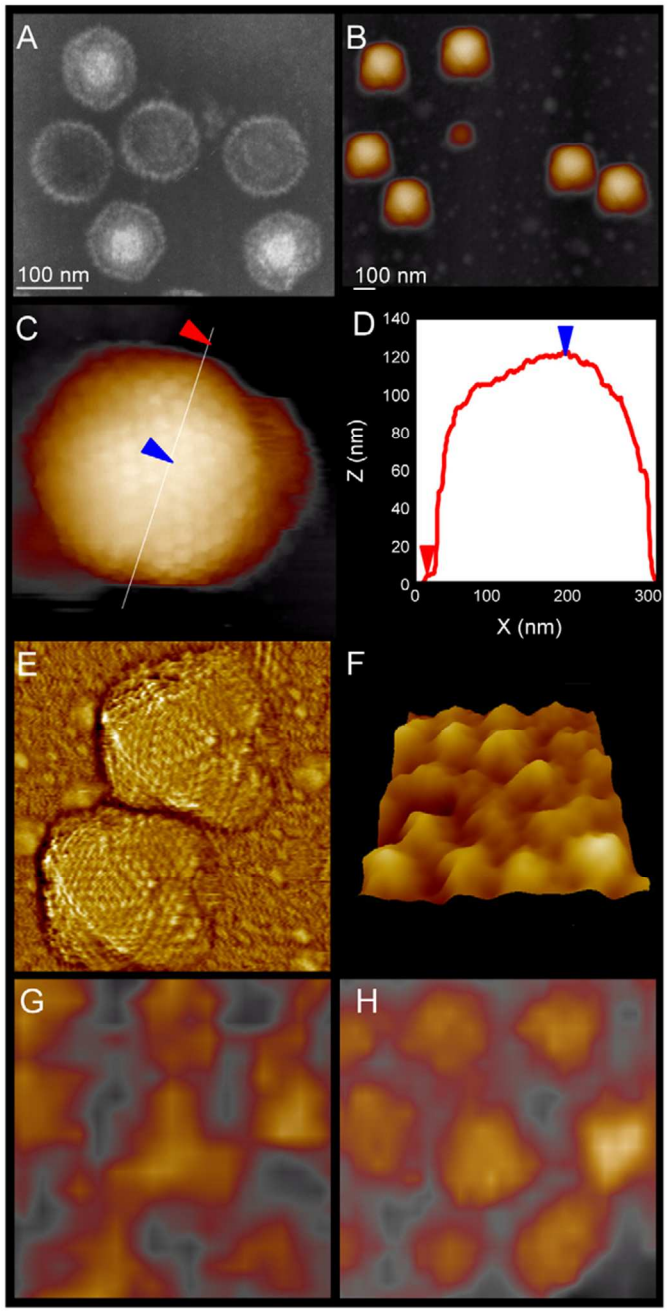

Figure 4 An electron microscopy image (**a**) and atomic force microscopy (AFM) intermittent contact mode topography image (**b**) of herpes simplex type 1 (HSV-1) virus capsids. **c, d** A high resolution topography image of an HSV-1 single virus capsid and the corresponding height profile. From the topography image (510 nm x 560 nm) in **e**, facets can be distinguished on the icosahedral-shaped capsid. A three-dimensional topography image (100 nm x 100 nm) in **f** illustrates that capsomeres can be resolved on the face of the capsid. Pentagonal and hexagonal arrangements of proteins can be distinguished from the AFM topography images (40 nm x 40 nm) in **g** and **h**, respectively. (Reprinted from ref. 122 with permission from the Company of Biologists, Ltd. doi: 10.1242/jcs.032284).

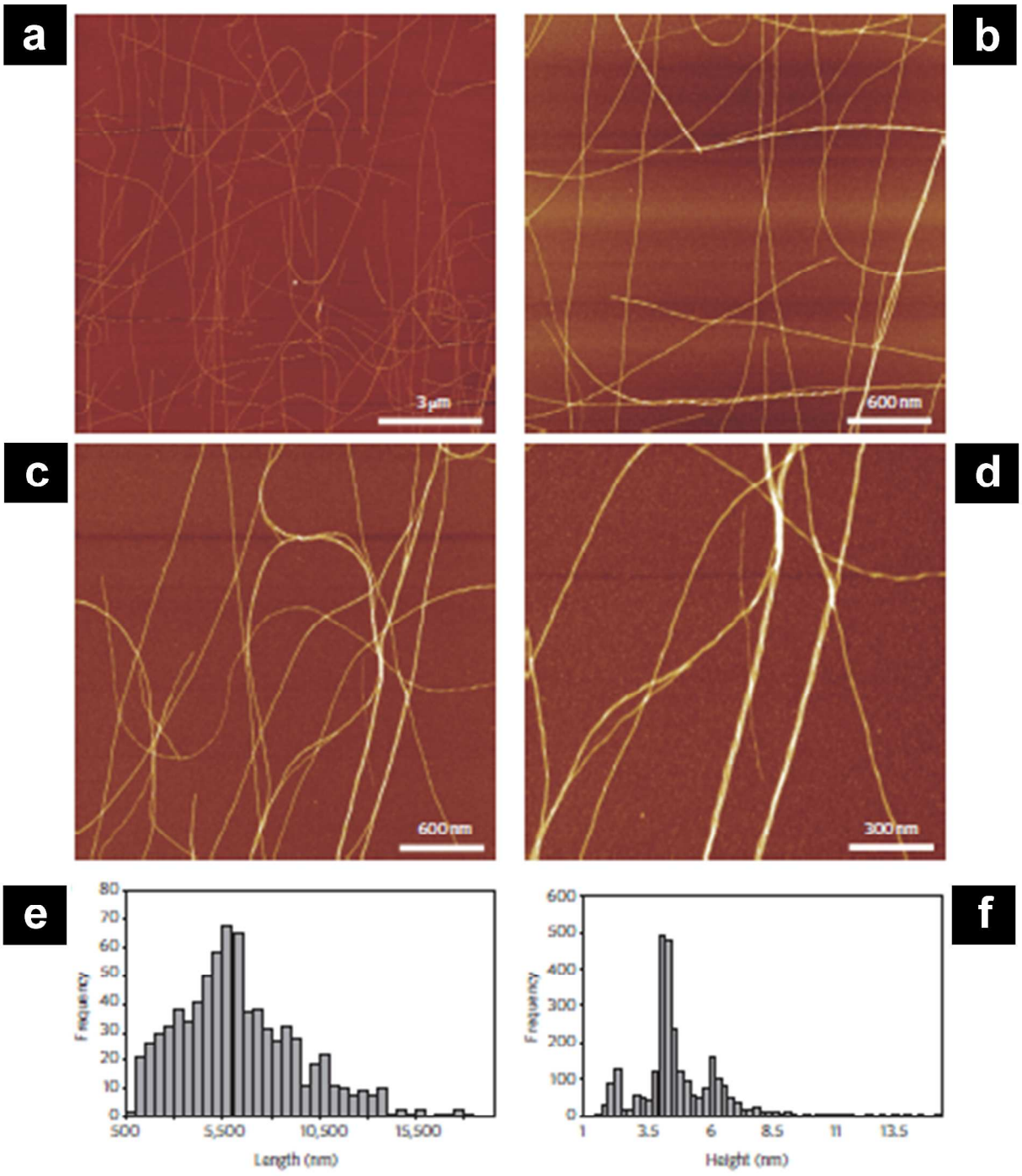

Figure 5 Atomic force microscopy (AFM) images at various magnifications of *β*-lactoglobulin fibrils acquired in intermittent contact mode (**a**-**d**). Histograms of fibril contour lengths (**e**) and maximum heights (**f**). (Reprinted from ref. 131 with permission from Nature Publishing Group. doi: 10.1038/nnano.2010.59).

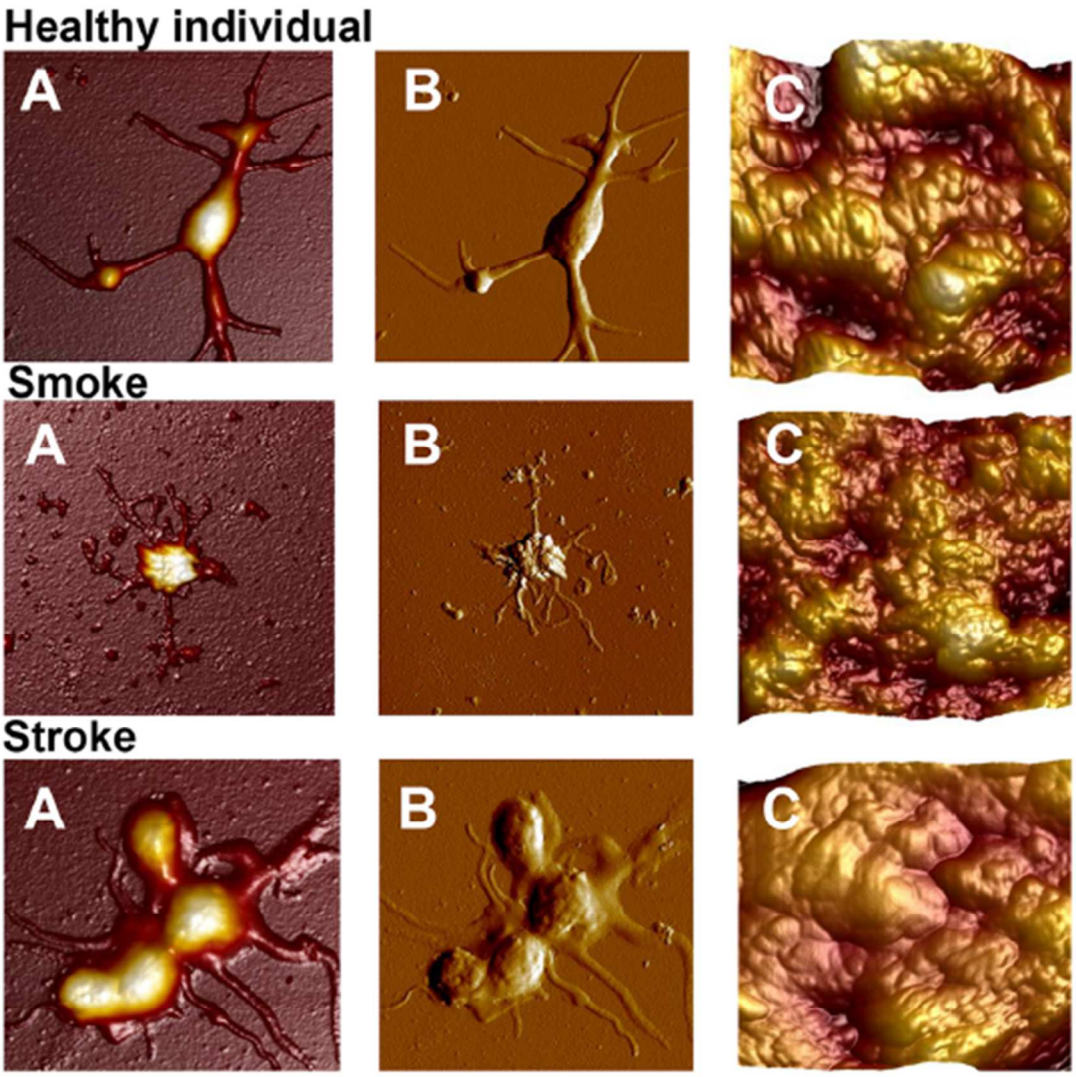

Figure 6a Atomic force microscopy topography images of blood platelets from healthy (**top**) smoker (**middle**) and stroke patients (**bottom**). x-y scale: 10 μm x 10 μm. z-scale: 1 μm. **b** Error images of blood platelets from healthy (**top**), smoker (**middle**) and stroke (**bottom**) patients. x-y and z-scales are the same as in **a**. **c** High resolution topography images of the platelet membranes from healthy (**top**), smoker (**middle**) and stroke (**bottom**) patients. x-y scale: 1 μm x 1 μm. z-scale: 0.2 μm. (Reprinted from ref. 80 under the Creative Commons Attribution (CC BY) license. doi: 10.1371/journal.pone.0069774).

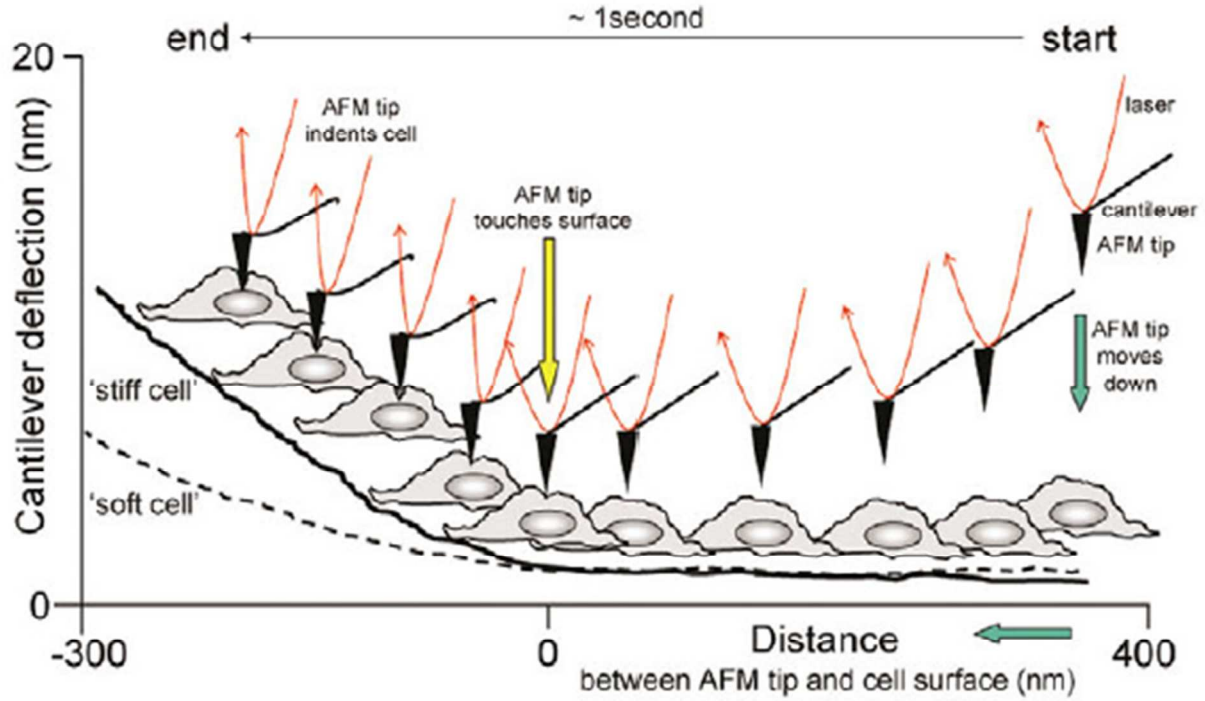

Figure 7 Artistic depiction of an atomic force microscopy force approach curve, which can be used to distinguish between stiff and soft cells. (Reprinted from ref. 156 with permission from the Company of Biologists, Ltd. doi: 10.1242/jcs.02886).

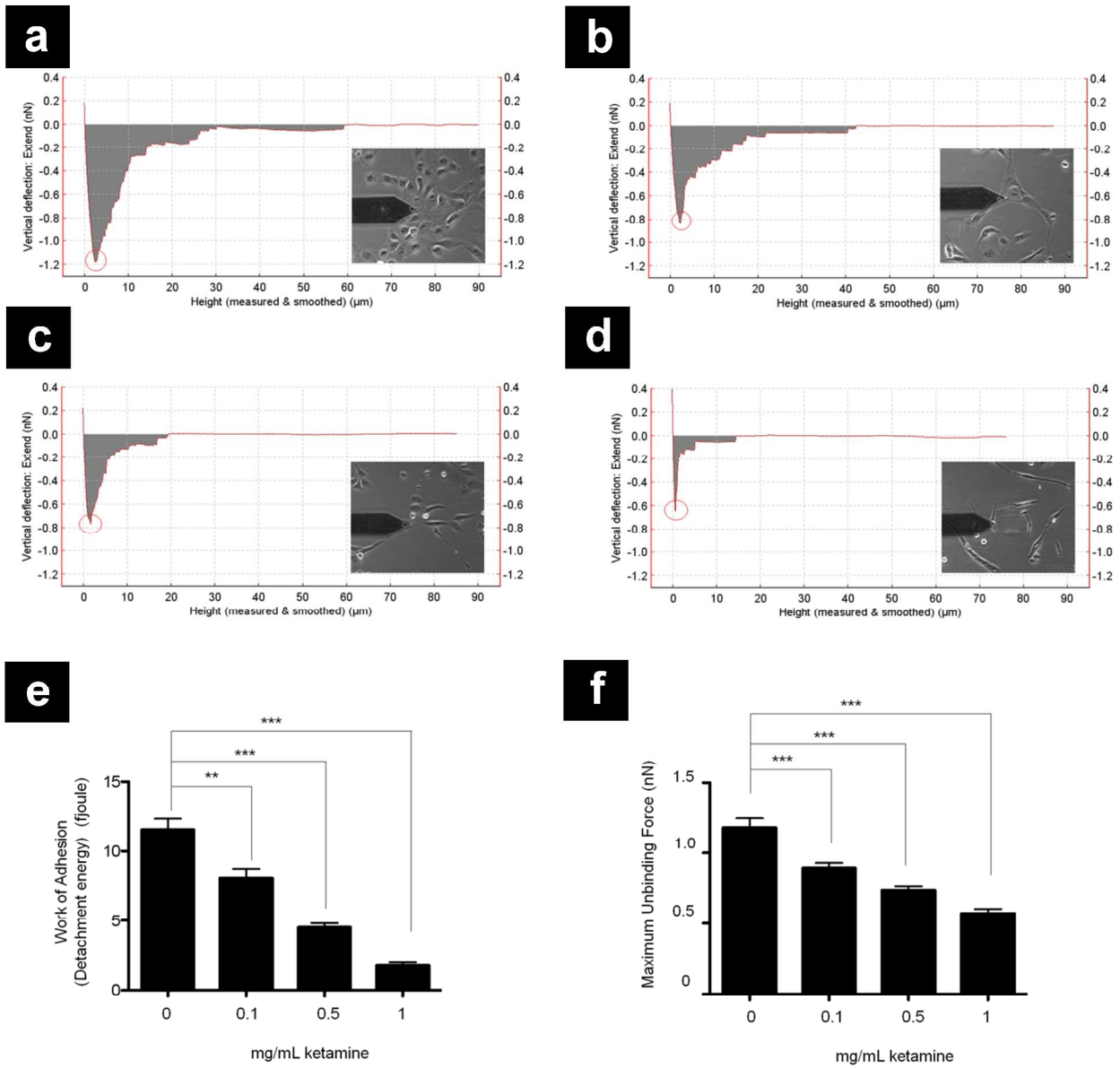

Figure 8 Single cell force spectroscopy retraction curves taken over human epithelial cells from the proximal tubule to study the effects of ketamine exposure (**a**-**d**). Force curves were acquired for cells exposed to 0, 0.1, 0.5 and 1 mg/mL of ketamine and results are shown in **a**, **b**, **c** and **d**, respectively. For these experiments, a single epithelial cell was attached to the AFM probe, prior to force curve acquisition, to study the unbinding force and maximum detachment energy between two single cells. Detachment energy was found via the integrated area under each retraction curve (gray area under curves in **a**-**d**). The maximum unbinding force (red circles in **a**-**d**) was found from the minimum of the retraction curve. Bar graphs of detachment energy and maximum unbinding force, shown in **e** and **f**, respectively, show trends for each ketamine treatment concentration. Error bars are from 4 separate experiments, where key significances are shown, **** *P<0.0001*. (Reprinted from ref. 172 under the Creative Commons Attribution (CC BY) license. doi: 10.1371/journal.pone.0071819).

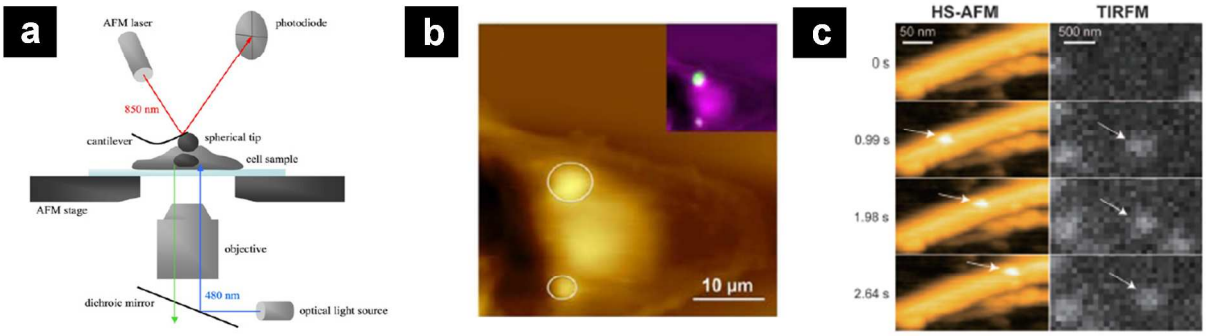

Figure 9a A schematic of a fluorescence microscopy-atomic force microscopy (FM-AFM) experiment, in which the AFM set-up is placed above the cellular sample and atop an inverted optical microscope. Fluorescence excitation and detection is achieved through an objective lens and a dichroic mirror. (Reprinted from ref. 196 with permission from the Institute of Physics. doi: 10.1088/0957-4484/20/17/175104) **b** An AFM topography image of a lung epithelial cell. Circles indicate possible sites of exocytosis of fluorescently-labeled lamellar bodies after chemical stimulation. The inset depicts a fluorescence microscopy image overlaid with the AFM topography image (now false colored purple), which illustrates that these protrusions in the lung epithelial cellular surface are from fluorescently-labeled lamellar bodies. (Reprinted from ref. 197 with permission from the American Chemical Society. doi: 10.1021/ac300775j) **c** Time-lapse high-speed AFM (HS-AFM) and simultaneously acquired total internal reflectance microscopy (TIRFM) images of a fluorescently-labeled chitinase A enzyme moving along a single chitin microfibril. Movement of chitinase A is indicated by white arrows in both HS-AFM and TIRFM images. Note that the field of view is different for the AFM and TIRFM images. (Reprinted from ref. 206 with permission from the American Institute of Physics. doi: 10.1063/1.4813280).

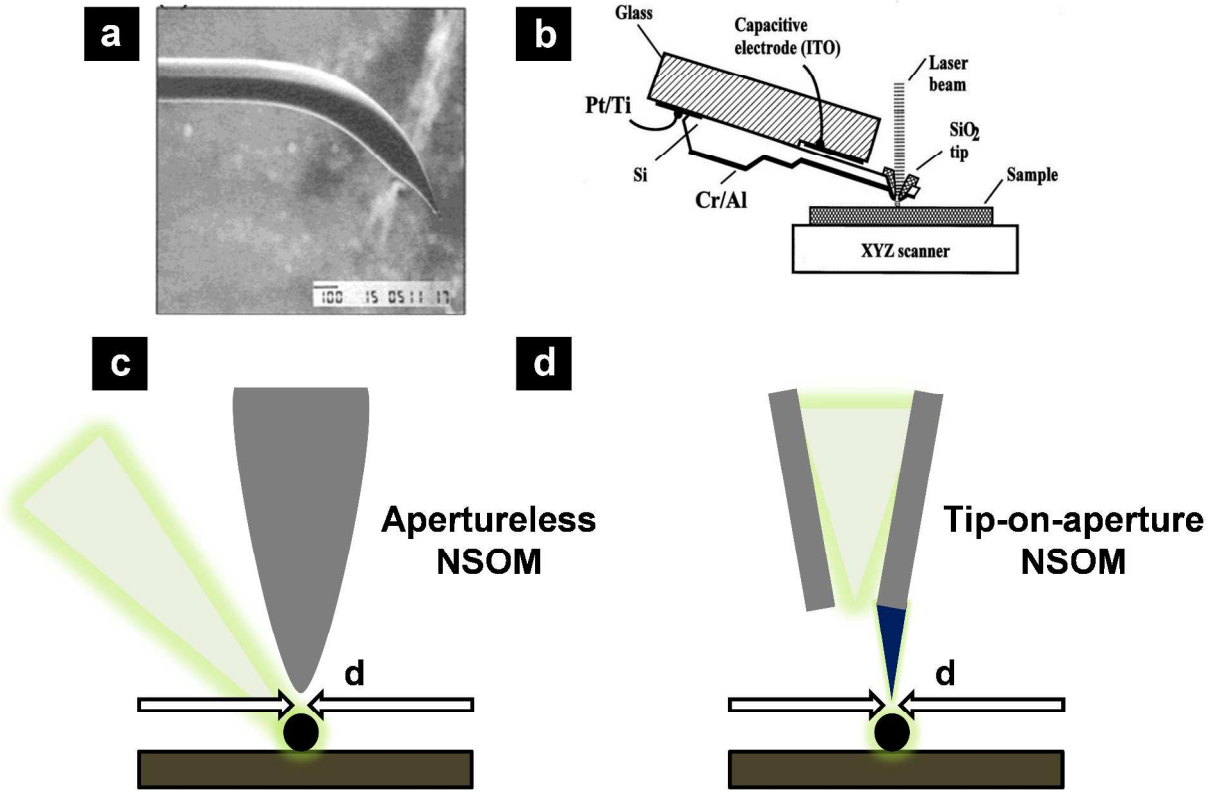

Figure 10a A scanning electron microscopy image of a bent, metallic-coated and etched optical fiber probe used in NSOM-AFM. The probe acts as the AFM probe and as the collector/illuminator. Feedback can be controlled via laser deflection off the back of the probe. (Reprinted from ref. 217 with permission from the American Chemical Society. doi: 10.1021/ac010536i). **b** An NSOM-AFM schematic that shows a Si microfabricated AFM probe containing an aperture. (Reprinted from ref. 218 with permission from the American Institute of Physics). **c** A schematic depicting a metallic AFM tip that is illuminated, at an angle, with light to cause an electric field enhancement at the tip. **d** A schematic that shows a tip-on-aperture probe for use in NSOM-AFM. Here, a sharp tip is placed outside an aperture, which enables operation in traditional NSOM illumination/collection mode and produces tip-induced field enhancement. In **c** and **d**, the letter 'd' represents the area of emitted light collection above the sample (small dot below arrows).

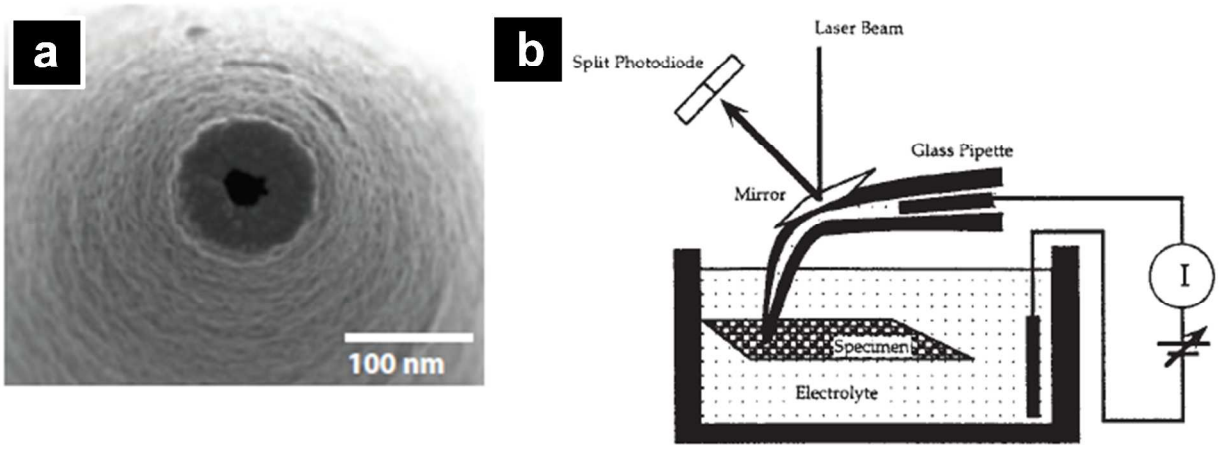

Figure 11a A scanning electron microscopy image of an end-on-view of a pulled nanopipette (~ 60 nm inner diameter). (Reprinted from ref. 227 with permission from Annual Reviews. doi: 10.1146/annurev-anchem-062011-143203). **b** A schematic of a scanning ion conductance microscopy-atomic force microscopy (SICM-AFM) experiment in which a bent nanopipette is used as both the force sensor and method to measure ion current while scanning the surface. The probe is controlled via laser deflection to a photodiode. (Reprinted from ref. 232 with permission from Wiley-VCH. doi: 10.1002/1097-0029(20010201)52:3<273::aid-jemt1013>3.0.co;2-m).

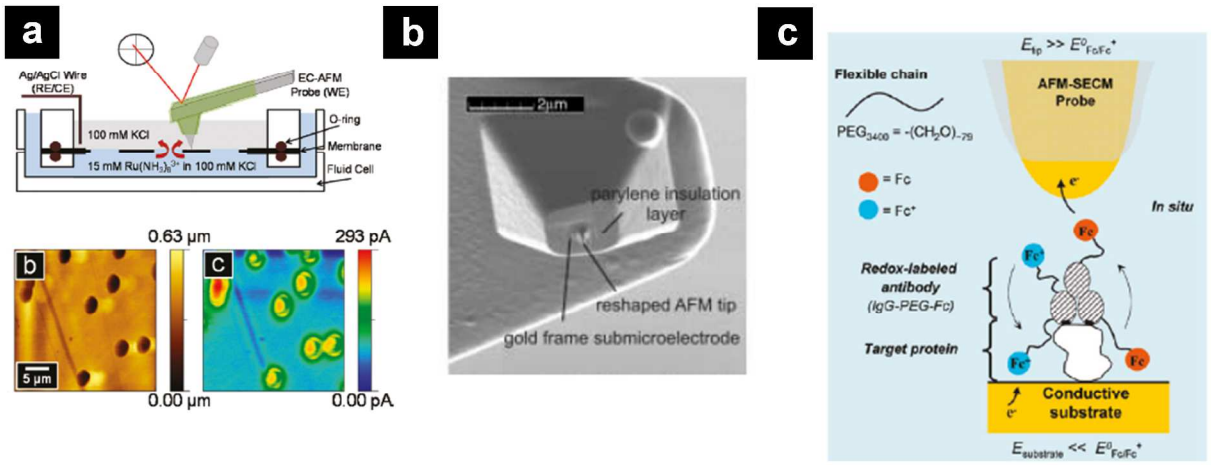

Figure 12a A schematic of a scanning electrochemical microscopy-atomic force microscopy (SECM-AFM) experiment where an AFM probe is measuring Faradaic oxidation or reduction current from an electroactive chemical species diffusing through a porous membrane (top image) while acquiring topographic data simultaneously. Topography of the porous membrane (**a**, lower left) and a correlated reduction current map (**a**, lower right) of the diffusing species. (Reprinted from ref. 252 with permission from the American Chemical Society. doi: 10.1021/la203032u). **b** A scanning electron microscopy image of a focus ion beam-milled AFM probe that is electrically insulated from a gold, frame-shaped electrode that is recessed from the AFM tip. (Reprinted from ref. 249 with permission from Wiley-VCH. doi: 10.1002/anie.200351111). **c** A schematic of a molecule-touching SECM-AFM (Mt/SECM-AFM) experiment, in which a gold SECM-AFM probe is depicted as an electron collector for molecules shuttled through redox-immunomarked proteins immobilized on a conducting surface. (Reprinted from ref. 275 with permission from the American Chemical Society. doi: 10.1021/ac201907v).

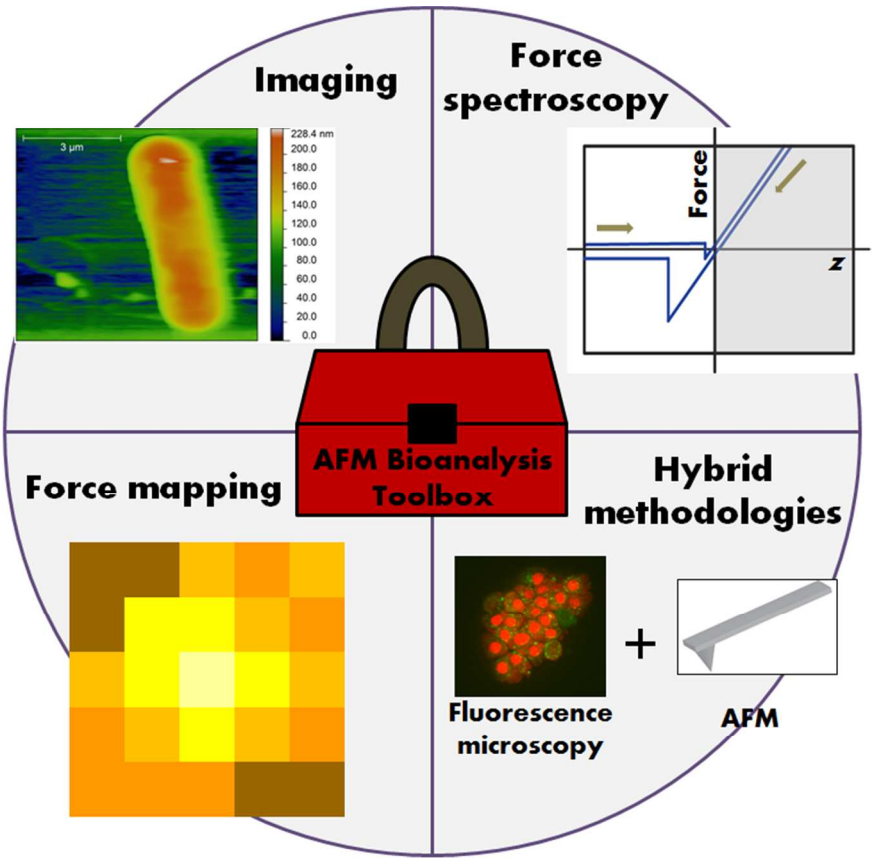

TOC Figure